ORIGINAL ARTICLE

The effect of process parameters on geometric deviations in 3D printing with fused deposition modelling

Cristian Cappellini[1] · Yuri Borgianni[1] · Lorenzo Maccioni[1] · Chiara Nezzi[1]

Abstract

Despite the large diffusion of additive manufacturing, and markedly fused filament fabrication, some quality aspects of the 3D printed parts have not been dealt with sufficiently. This applies particularly to geometric accuracy and the influence process parameters have on it. The paper describes an experiment in which 27 copies of a part were manufactured by means of a desktop fused filament fabrication device while manipulating layer thickness, printing speed, and number of contours. The effect of such process parameters on five typologies of geometric deviations and the duration of the printing process was assessed. While all the process parameters showed effects on both the printing time and some geometric deviations, the number of contours resulted as the most critical factor. The paper includes a proposal to optimize geometric accuracy and the rapidity of the process, which foresees the maximization of the number of contours, the minimization of the layer thickness, and the use of an intermediate value for printing speed.

1 Introduction

Fused filament fabrication, commonly indicated with the commercial name fused deposition modelling (FDM), is an additive manufacturing (AM) technology used to print parts that are often characterized by geometrically complex shapes [1, 2]. FDM is typically considered a reference process for rapid prototyping (RP) [3]. Nevertheless, this technology is evolving continuously and rapidly. FDM-printed parts are no longer used for esthetic prototypes and displays only, but also as end products. Examples include drilling grids in the aerospace industry [4], foot prostheses [5], and edentulous mandible trays [6] in the bio-medical field. It is evident

that these products require specific performances. Performances to be attained typically concern mechanical properties, surface finish, defects, and other quality-related aspects. Much research considers a subset of these performances to limit the complexity of presented studies. Consistently, the authors dedicate here special attention to quality and, markedly, geometric accuracy, as explained and motivated in the following section.

Generally, to cope with quality requirements, the optimization of process parameters is of paramount importance. This is clearly not limited to FDM process [7, 8], but it extends to other AM techniques, such as powder bed fusion [9, 10], or wire and arc additive manufacturing [11, 12]. The effects of process parameters have been investigated to identify the most impacting ones and their relations to performance measures [13–21]. Despite these numerous attempts, the production of functional parts with FDM is still limited due to the limited accuracy of prints if compared with traditional manufacturing process like turning and milling. Xinhua et al. [22] is a case in point in this regard.

The study of Mohamed OA et al. [23] is a first attempt to summarize the studied relations between process parameters and product performance measures in FDM, but other studies have followed its publication. Section 2 extends the

✉ Cristian Cappellini
cristian.cappellini@unibz.it

Yuri Borgianni
yuri.borgianni@unibz.it

Lorenzo Maccioni
lorenzo.maccioni@unibz.it

Chiara Nezzi
chiara.nezzi@unibz.it

1 Faculty of Science and Technology, Free University of Bolzano, Piazza Università 1, 39100 Bolzano, Italy

review of the effect of process parameters on quality performances and the duration of the 3D-printing process, which is a plainly connected aspect. The extension of the review sheds light on the limited attention paid to geometric accuracy. This takes place despite geometric accuracy is expected to play an important role in objects created through FDM. On the one hand, FDM ambition to become a commonplace technology for functional products determines the need to cope with quality aspects that, inherently, include geometric accuracy. On the other hand, limiting geometric deviations can be seen as a prerogative for RP too. Geometric issues are supposed to affect esthetics [24] and perceived quality of parts [25], with a potential detrimental effect on design decisions following the RP stage.

The overall scope of the paper is therefore to acquire more knowledge about the role played by process parameters on geometric accuracy. As process duration is a known issue in AM (and even more markedly in FDM) and accuracy goals are typically offset by the extension of the printing time (*PT*), the latter is considered contextually in this study. The specific objective of the paper is then a proposed optimization of geometric accuracy and *PT*.

The residual of the paper is organized as follows. Section 2, beyond contributing to the understanding of the studied effects of process parameters on quality features and process duration, specifies the methodological objectives. In particular, manipulated process parameters and tested geometric deviations are selected. Section 3 illustrates the methodological procedure followed to obtain the data necessary to pursue the paper's objective. While results are presented and discussed in Sect. 4, conclusions are drawn in Sect. 5.

2 Background

By considering [23] as a starting point to identify pertinent contributions and common process parameters, the literature review was expanded to stress the attention paid to this topic. The focus of the authors' review included the typology of relations between process parameters and investigated affected factors. The outcome is a table (Table 1) that shows the core relations between process parameters (first column), and product/process performances (first row). The definition of the former within FDM is taken for granted; readers can benefit from [26] for clarifications. The latter are defined with a positive acceptation to indicate the desirability of the effects, hence as follows:

- Surface finish instead of roughness
- Dimensional and geometric accuracy instead of deviations or errors
- Process speed instead of *PT*.

The cells of Table 1 report the sources that have analyzed the relation between the former and the latter. Relations are classified as follows:

- Positive (direct) if the increase of the process parameter results in a statistically significant improvement of the performance measure. This kind of relationship is marked by its arrangement in the respective sub-column featured by an upwards arrow.
- Negative (inverse) if the increase of the process parameter results in a significant worsening of the performance measure. This kind of relationship is marked by its arrangement in the respective sub-column featured by a downwards arrow.
- Neutral if the tested relationship was neither significantly positive nor negative. This kind of relationship is marked by its arrangement in the respective sub-column featured by a dash.

As readers can notice, studies have given rise to different, if not conflicting, results. This might take place because the relation between process parameters and accuracy is possibly mediated by materials, geometry, or other factors. For instance, a plain contradiction concerns the influence of raster width on surface finish. An increase of raster width (obtained through a variation of material flow rate) from 0.3 to 0.5 mm improves the surface finish of the printed piece [27]. Conversely, [28] states that by increasing the raster width (0.4 mm, 0.53 mm, 0.66 mm), the surface finish worsens.

The attention paid to geometric accuracy is hitherto limited. Among the few contributions, [35] shows that specific dimensional and geometric accuracy performances can be attained by acting on nozzle temperature, layer thickness (*LT*) and infill density. Similarly, [36] analyzes the geometric accuracy of circular features, concluding that different process parameters, such as raster angle and air gap, can strongly influence local dimensional deviations over circumferences and diameters. In [56], the scholars customized the design of a test sample to measure key features of the components quantifying the effect of some process parameters (e.g., *LT*, extruder temperature, and infill density) on the geometric accuracy resulting by the process. They finally found an optimal combination of these parameters. Another contribution was made by [59], which proposes a detailed analysis of the effects of layer cooling time on a part's geometrical deviations. The contribution further discusses the overall printing speed (*PS*) and issues concerning the extruder's temperature. Eventually, [60] compares printed and machined holes in specimens, investigating the effects of standard process parameters on dimensional and geometric deviations.

Table 1 Summary of the relationships between process parameters and performance measures

Performance measures / Process parameters	Surface finish			Dimensional accuracy			Geometric accuracy			Process speed		
	↑	-	↓	↑	-	↓	↑	-	↓	↑	-	↓
Layer thickness (*LT*)		[13] [14]	[15] [16] [27] [29] [30] [32] [38] [44] [46] [50] [53] [55] [56] [57] [58] [61]		[16] [21] [22] [40] [47]	[7] [16] [17] [19] [20] [23] [27] [43] [51] [52] [53] [54] [57] [61] [62] [64]		[56]	[35]	[28] [30] [32] [33] [34] [41] [50] [57]	[13] [23] [31] [39]	
Raster width	[27] [61]	[15] [57]	[28]		[21] [22] [27] [40] [43] [48] [57] [61]	[17] [18] [19]					[23] [33]	[41]
Build orientation angle	[38] [44] [45] [61]	[14] [15] [16] [28] [37]	[57] [60]	[51] [61]	[16] [17] [18] [52]	[45] [57] [60]				[41] [57]	[13] [23] [33] [42]	
Raster angle	[27]	[14] [28]		[18]	[17] [27] [36] [43] [52] [64]					[41]	[23] [32] [33] [57]	
Raster-to-raster air gap		[27] [28] [38]			[17] [18] [27] [40]			[36]		[41]	[23]	[28] [32]
Infill density	[45] [46]	[16] [55] [57]		[45]	[16] [22] [47] [54] [57] [62]	[51]	[35]	[60]			[31]	[57]
Printing speed (*PS*)	[29]	[15]	[55] [57]	[18]	[21] [22] [47] [54] [58]	[19] [57] [59] [62]		[59]		[50]		

Table 1 (continued)

Performance measures Process parameters	Surface finish			Dimensional accuracy			Geometric accuracy			Process speed		
	↑	-	↓	↑	-	↓	↑	-	↓	↑	-	↓
Nozzle temperature	[46] [63]	[38] [61]	[57]		[22] [47] [63]	[20] [41] [49] [53] [54] [57] [58] [59] [61]	[56] [60]	[35] [59]			[57]	
Number of contours (*NC*)			[57]			[23] [57]					[23] [31]	
Contour width		[38]		[40]		[52]					[33]	[28] [41]

Beyond the limited consideration of geometric accuracy in FDM studies, it is worth noting that available studies have failed to address to what extent the achievement of geometric quality can be counterbalanced by *PT*. In order to fill this gap, the authors have designed and conducted an experiment, as made apparent in Sect. 3.

The first step was to select some process parameters for the scopes of the experiment. With the aim to identify significant parameters, some were chosen from previous studies giving rise to no conflicting outputs and that could logically affect geometric properties of 3D-printed parts and, contextually, the duration of the printing process. The listed parameters below are characterized by a strongly uneven popularity (high, average, low) in previous studies.

- *LT* is the most studied parameter according to Table 1. Its impact on performance measures and process speed is straightforward in many studies. *LT* is a good candidate for affecting geometric quality because of its recognized role in the staircase effect of 3D-printed parts, e.g., [65].

A few studies have already considered this parameter in relation to geometric accuracy, but *PT* was never considered contextually.

- *PS* is possibly relevant when the accurate deposition of material is requested. The magnitude of its influence on process speed has been surprisingly overlooked based on Table 1.
- Number of contours (*NC*) can be crucial when it comes to the accuracy of external surfaces. Its effect on process duration has emerged as marginal so far.

The geometric deviations that will be addressed in this paper are selected for convenience and reported in Table 2 along with their definition based on the standard 1SO 1101:2017 [66] about geometrical product specifications. Despite the peculiarities of AM technologies, the ISO 1101 has still to be considered when it comes to geometric dimensioning and tolerancing (GD&T) following ASME Y14.46 [67], as reported in [68, 69].

Table 2 Summary of the geometric deviations selected for this study

| Name of the geometric deviations	Brief explanation
Flatness	Minimum distance between two parallel planes defining a region of space which entirely contains the reference surface.
Cylindricity	Minimum (radial) distance between two coaxial cylinders defining a region of space which entirely contains the reference surface.
Concentricity	Minimum diameter of a cylinder having its axis parallel to a datum that defines a region of space which entirely contains the axis of reference cylindrical surface.
Surface parallelism	Minimum distance between two parallel planes (parallel to a datum) defining a region of space which entirely contains the reference surface.
Surface perpendicularity	Minimum distance between two parallel planes (perpendicular to a datum) defining a region of space which entirely contains the reference surface.

3 Materials and methods

In order to understand how the three selected parameters affect geometric deviations, a set of parts characterized by different process parameters was printed and hereafter measured with a coordinate measuring machine (CMM) through a developed automatic measuring procedure. The choice and design of the specimen are justified in the subsection that follows. Subsequently, the printing and measuring processes are described.

3.1 Design of the part

As no standard shapes are used in the study of geometric deviations for AM technologies, a part has been designed, which lent itself to the assessment of all the geometric deviations reported in Table 2. The part has been designed with the following features (Fig. 1):

- A cylinder at the base of the piece (C1).
- Two concentric holes with a cylindrical shape and different diameters (C2 and C3) that are theoretically concentric even with C1.
- Eight surfaces perpendicular to C1 (S1, S2, S3, S4, S5, S6, S7, S8) arranged as a regular octagon.
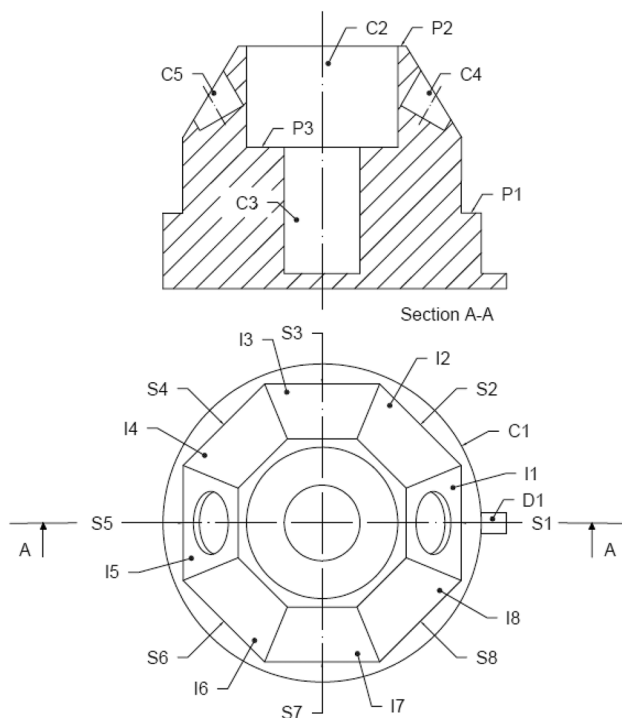
Fig. 1 2D CAD model of the part to be printed (top view and sectioned front view); it includes feature codes used in the above dot list

- Eight surfaces inclined at 30° with respect to S-surfaces (I1, I2, I3, I4, I5, I6, I7, I8).
- Two inclined (at 30° with respect to the C1–C3 axis), symmetric holes with a cylindrical shape (C4 and C5) respectively on the surfaces I1 and I5.

A complete draft of the part including dimensions can be found in Appendix Fig. 33.

In this way, it has been possible to obtain features with different orientations and thus mitigate any possible effect of the building orientation. Horizontal, vertical, and inclined surfaces have been conceptualized for both planar and cylindrical surfaces so to avoid the need of support material. Moreover, the horizontal surfaces have been conceived with different heights in order to attenuate any influence of the distance from the printing plane.

To avoid the use of support material, no horizontal holes were included in the part, and the inclination of surfaces I1–I8 and holes C4–C5 are limited to 30° from the vertical direction. Two inclined holes only were made in order not to reduce the surface area of the I1–I8 surfaces excessively and, therefore, not to compromise their measurement. The little "bulge" (feature D1) made on C1 near the printing plane is a reference that facilitates the consistency of the measurement operations by identifying the correct faces.
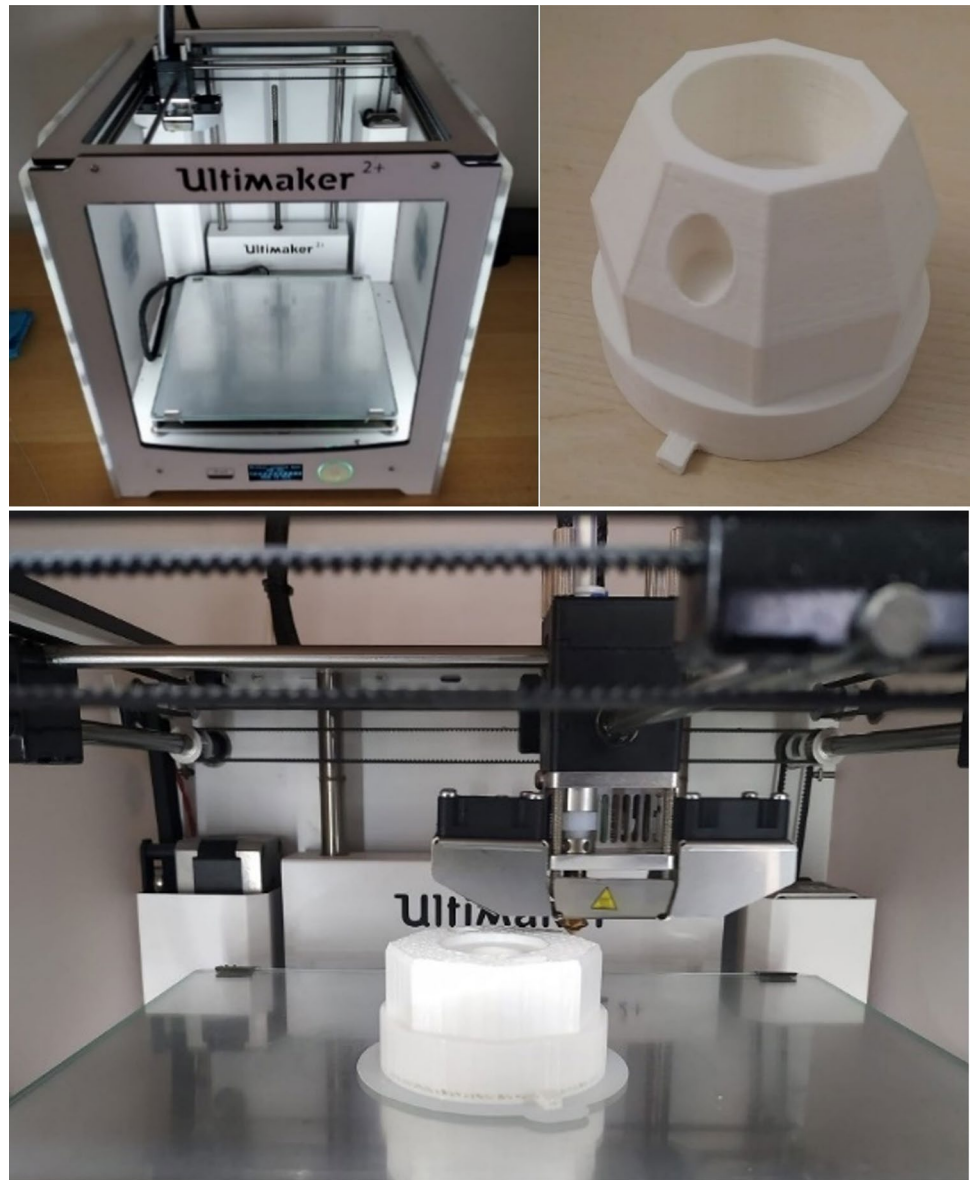
3.2 Printing process

In the present study, a single filament Ultimaker 2 + printer (located at the Bitz Fablab of the Free University of Bozen-Bolzano) was used (Fig. 2). The detailed printer specifications are shown in Table 3.

All parts were printed with an infill density of 20% with a grid pattern; the utilized material is a common white filament of PLA for a 0.4-mm diameter nozzle.

A set of control levels has been assigned to each of the three process parameters (i.e., *LT*, *PS*, and *NC*); the selected values for each parameter are reported in Table 4. The process parameters have been set to achieve a low, medium, and high value in accordance with the capabilities (and reasonable operating ranges) of the used 3D printer.

The number of objects to be printed was given by all the possible combinations considering the three levels and the three parameters. Therefore, in order to conduct a fully factorial experiment, the number of pieces to be printed was $3^3 = 27$. Table 5 reports the different values for the parameters and the levels assigned. It is evident that every piece corresponds to a unique combination of the selected parameters. Table 5 includes the *PT* for each combination.

Fig. 2 Ultimaker 2+, printing process, and one of the printed parts

3.3 Measuring process

In order to detect geometric deviations among the 27 FDM-ed parts, they were measured by means of a CMM (Coord 3 Ares NT), located in the Mechanical Lab of the

Table 3 Printer specifications

Ultimaker 2+ specifications	
Printing technology	Fused deposition modelling (FDM)
Printing bed size	223 × 223 × 205 mm
Nozzle diameter	0.40 mm
Material	PLA
Filament diameter	2.85 mm
Print head	1 (Swappable nozzle)

Free University of Bozen-Bolzano (Fig. 3). The machine is equipped with a PH10 5-axis touch-trigger system. The workstation is furnished with a desktop computer equipped with the Coord 3 metrology software TouchDMIS, utilized to digitally record measurements.

Furthermore, the measuring process was supported by a bespoke clamp designed for correct positioning of the

Table 4 Process parameters and control levels

Parameters	Layer thickness [mm]	Printing speed [mm/s]	Number of contours [#]
Low	0.16	72	1
Medium	0.20	90	2
High	0.24	108	3

Table 5 The 27 different combinations of parameters for 3D printed parts

Test (part)	Layer thickness [mm]	Printing speed [mm/s]	Number of contours [#]	Printing time [min]
1	0.16	72	1	179
2	0.16	72	2	198
3	0.16	90	1	149
4	0.16	90	2	165
5	0.16	72	3	218
6	0.16	108	1	130
7	0.16	108	3	157
8	0.16	90	3	181
9	0.16	108	2	143
10	0.20	90	2	134
11	0.20	90	1	121
12	0.20	72	2	160
13	0.20	72	1	145
14	0.20	90	3	146
15	0.20	108	2	116
16	0.20	108	3	127
17	0.20	108	1	105
18	0.20	72	3	176
19	0.24	108	3	105
20	0.24	108	1	87
21	0.24	72	3	146
22	0.24	72	1	120
23	0.24	108	2	96
24	0.24	90	3	121
25	0.24	90	2	110
26	0.24	90	1	100
27	0.24	72	2	133

parts to be inspected. This clamp prevents undesired movements of the piece during the measuring process. Moreover, it eases the positioning of parts with consistent orientation (due to the bulge, as aforementioned). This results in speeding up the process of alignment and, therefore, starting the automatic measuring procedure. Pictures of the support clamp are included in Fig. 4.

After an initial alignment of the coordinate systems of the part and the touch probe by manual probing of plane P2, cylinder C2, and surface S3, the automatic procedure was set. This allows an automatic measuring mode to take place. The measuring procedure had to ensure appropriate coverage for all the surfaces to be measured. More in detail, the procedure foresaw the automatic acquisition of a certain number of points with the touch probe for every surface to be studied; the number of detected points indicated below follows common practices and rules of thumb.

- Vertical surfaces are usually sufficiently described by 10 points each (surfaces S1 to S8).
- Inclined surfaces are usually sufficiently described by 15 points each (surfaces I1 to I8).
- Cylindrical features are sufficiently described by a minimum number of 12 points each to a maximum number of 36 points each, depending on their orientation and dimensions: hence, cylinders C4 and C5 were measured by acquiring 12 points each, cylinders C2 and C3 by acquiring 20 points each, and C1 by acquiring 36 points.
- Horizontal planes are commonly established by acquiring 10 points each (planes P1 to P3).

The measurement process took place after the complete setting of this automatic procedure on the aforementioned software of the CMM. The time interval required for a single whole procedure was approximately 10 min per part. The geometric deviations measured for the several part features are reported in Table 6.

4 Results and discussion

4.1 Statistical analysis of geometric deviations data

Consistently with Table 2, the extracted data are in terms of geometric deviations—hence, the larger the values, the worse. In the same manner, the effect of the analyzed process parameters will be considered as positive if it concerns a reduction of the geometric deviation, while as negative if involving an increase of the latter. In relation to the geometric deviations reported in Table 6, and with the aim to investigate how these are influenced by the selected process parameters, the experimental results have been statistically analyzed through ANOVA techniques. In particular, still with respect to Table 6, the variables are as follows:

- $FLAT_P$, $FLAT_S$, and $FLAT_I$ are related to the flatness of horizontal surfaces P, vertical surfaces S, and inclined surfaces I respectively;
- CYL_C represents the cylindricity;
- $CONC_{CxCy}$ indicates the concentricity of the circular feature x with respect to y;
- PAR_{PxPy} and PAR_{SxSy} describe the parallelism among horizontal surfaces Px and Py, and vertical surfaces Sx and Sy respectively;
- $PERP_{SxP1}$ indicates the perpendicularity of the vertical surface Sx with respect to the horizontal surface P1.

All the measurements of the geometric deviations are reported in the tables in Appendix Tables 21, 22, 23, 24, 25, 26, 27, and 28.

Fig. 3 Lab workstation
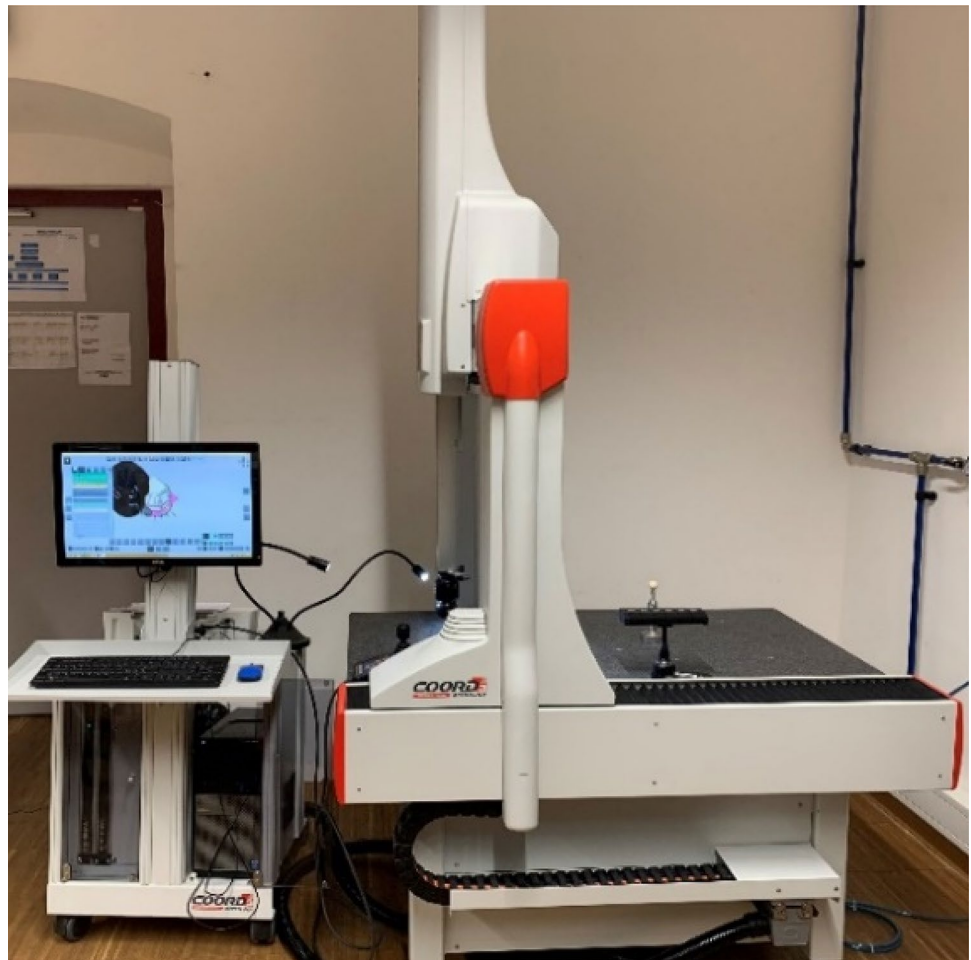
4.1.1 Flatness of horizontal surfaces

As visible in Fig. 1 and understandable from Table 6, each test, corresponding to a determined printed part, is characterized by having more than a single feature correlated to the analyzed geometric deviation. By considering, for example, the flatness of the horizontal surfaces, each specimen includes three related features, namely $FLAT_{P1}$, $FLAT_{P2}$, and $FLAT_{P3}$. The objective of this work is to evaluate the influence of the process parameters variation on a determined geometric deviation (e.g., $FLAT_P$), but independently from the printed feature (e.g., without considering if the affected flatness is the one related to surface P1, or P2, or P3). In this regard, if the measured geometric deviation is not affected by the particular feature itself (e.g., by its position, or its orientation with respect to the print platform, or its extension), every measure of a particular geometric feature can be considered as a test repetition. As regards again the flatness of horizontal surfaces, for example, it is possible to assess that, 27 tests, by varying three process parameters on three levels, have been performed with three repetitions

(P1, P2, and P3), for a total of 81 acquired measurements, as in Appendix Table 21.

In order to analyze of the effects of the process parameters on the geometric deviations rigorously, the normal distribution of the acquired data must be satisfied. For verifying the normality assumption, the residuals of the examined data are plotted on a probability plot in which the x-axis represents the residuals, and the y-axis expresses their normal probability percentage. Figure 5 depicts the probability plot, resulting from the normality test, for the measured $FLAT_P$. The red dots symbolize the acquired data; the central line corresponds to the cumulative probability; the two external curves represent the 95% confidence interval (CI) boundaries, which is a typical value employed in the practice [70].

If the normality assumption is verified, and consequently the statistical analysis of the input parameters influence has significance, the results in the probability plot are close to the central line and restricted between the CI curves. By this consideration, Fig. 5 shows a lack of normality of the reported $FLAT_P$ data. As described in [71], a lack of normality in the data can be generally due to two different

Fig. 4 Support clamp fastened to the CMM together with a constrained 3D-printed part
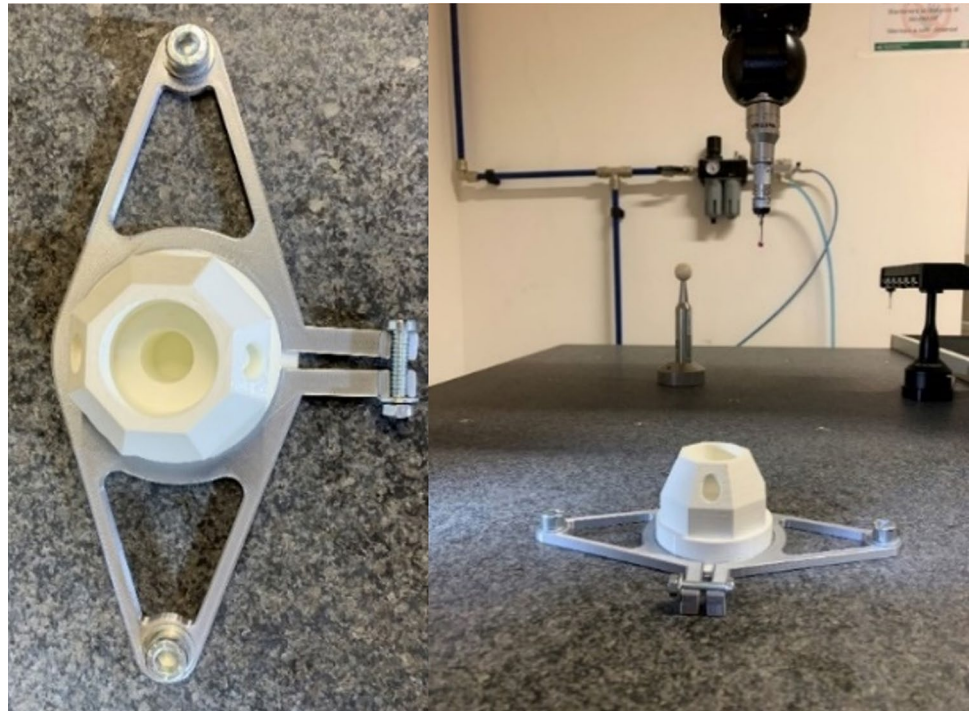
conditions: an effective absence of normality of the data, or to the presence of outliers. The latter are mostly caused by calculation or data coding mistakes and are characterized by a high value of the standardized residuals. The distinction between these conditions is difficult, since it relates to several factors, such as the measurer's experience, and the randomization and sequence of the measurements [71]. In any case, it is possible to remove the data having standardized residuals bigger than 3 or 4 times the standard deviation, and checking again the normality of the remaining set of data, without compromising the reliability of the ANOVA results [71].

Table 6 List of all the measured geometric deviations

Geometric deviations	Name	Part feature	Results Appendix Tables 21 to 28
Flatness	$FLAT_P$	P1–P3	Table 21
	$FLAT_S$	S1–S8	Table 22
	$FLAT_I$	I1–I8	Table 23
Cylindricity	CYL_C	C1–C5	Table 24
Concentricity	$CONC_{C1C2}$	C1 with respect to C2	Table 25
	$CONC_{C1C3}$	C1 with respect to C3	''
	$CONC_{C2C3}$	C2 with respect to C3	''
Surface parallelism	PAR_{P1P2}	P1 with respect to P2	Table 26
	PAR_{P1P3}	P1 with respect to P3	,,
	PAR_{P2P3}	P2 with respect to P3	,,
	PAR_{S5S1}	S5 with respect to S1	Table 27
	PAR_{S6S2}	S6 with respect to S2	,,
	PAR_{S7S3}	S7 with respect to S3	,,
	PAR_{S8S4}	S8 with respect to S4	,,
Surface perpendicularity	$PERP_{S1P1}$	S1 with respect to P1	Table 28
	$PERP_{S2P1}$	S2 with respect to P1	''
	$PERP_{S3P1}$	S3 with respect to P1	''
	$PERP_{S4P1}$	S4 with respect to P1	''
	$PERP_{S5P1}$	S5 with respect to P1	''
	$PERP_{6xP1}$	S6 with respect to P1	''
	$PERP_{7xP1}$	S7 with respect to P1	''
	$PERP_{8xP1}$	S8 with respect to P1	''

**Fig. 5** Probability plot of *FLAT_P* (in μm) resulting from normality test
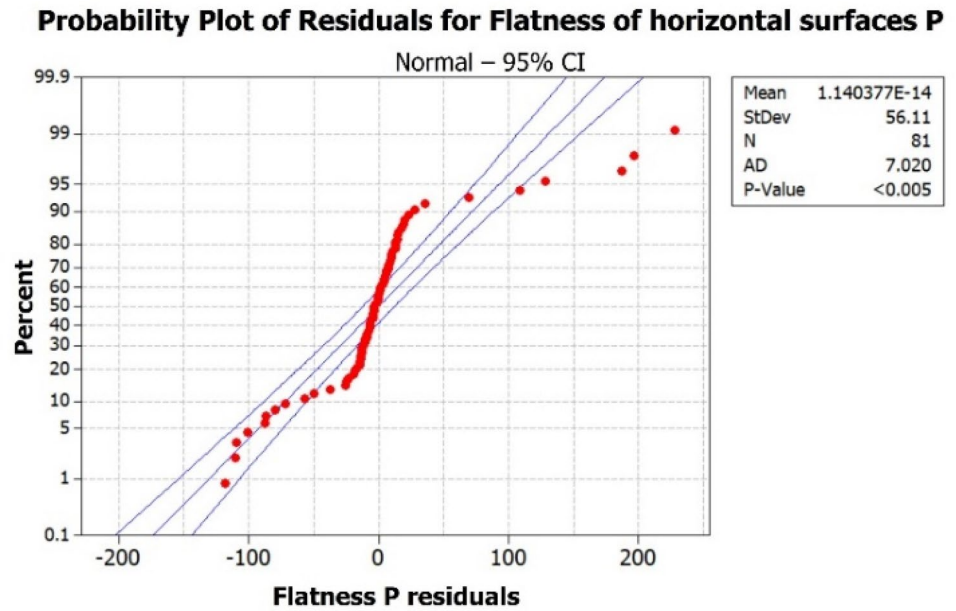
A preliminary ANOVA of the data related to flatness of horizontal surfaces highlighted the presence of 9 outliers with standardized residual values, such that they can be eliminated. More in detail, the identified outliers are relative to tests 16 and 17 for the surface P1, and tests 10, 12, 15, 19, 20, 22, 26 for the surface P3. The distribution of the outliers does not underline any correlation between them and the process parameters' values. It can be observed, instead, that most of the outliers are related to the acquired measurements on surface P3, and this can be due to the increased difficulty in the CMM's measuring of such a deep and internal feature.

The normality test of the remaining $81 - 9 = 72$ measurements led to the probability plot of Fig. 6. The normal distribution of the data in the absence of outliers is clearly identifiable; hence, performing the ANOVA on this set of data will provide reliable information about the influence of the process parameters on $FLAT_P$.

The results of the ANOVA for $FLAT_P$ are reported in Table 7. The first column, named "Source," shows the considered process parameters, i.e., *LT*, *PS*, and *NC*. It is possible to notice that, in addition to the influence of the single process parameter on the response (in this case

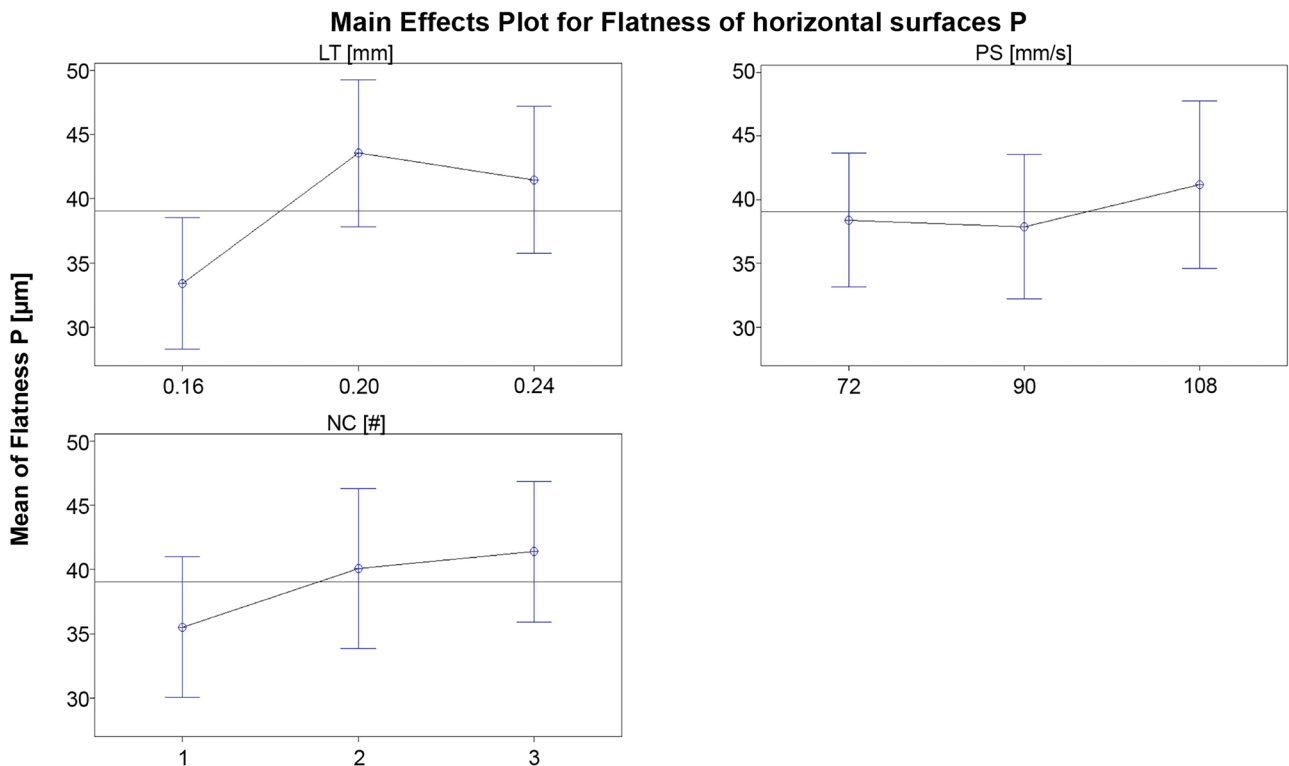**Fig. 6** Probability plot of *FLAT_P* (in μm) resulting from normality test without outliers
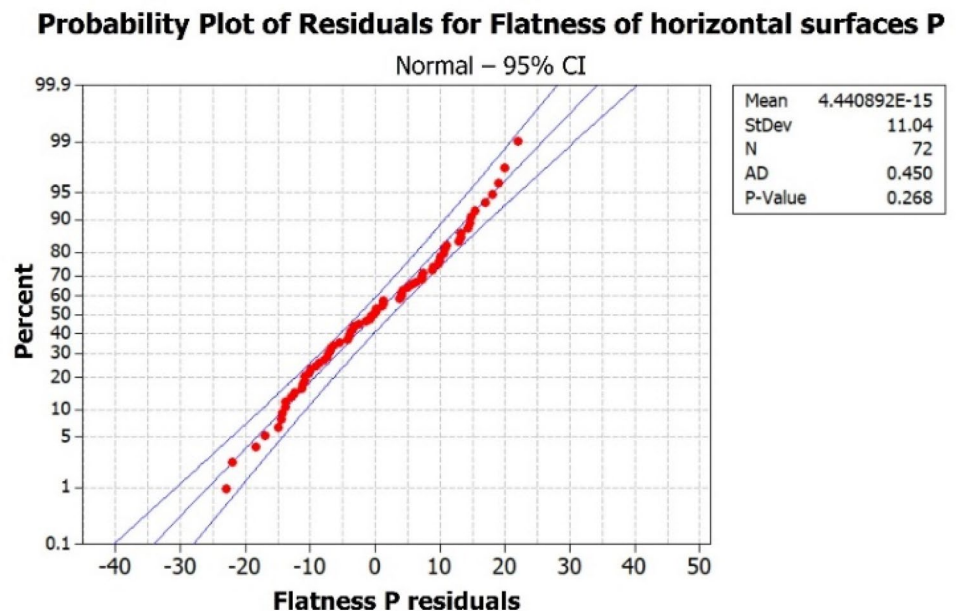
Table 7 ANOVA for $FLAT_P$

Source	DOF	Seq SS	Adj SS	Adj MS	F	p
LT	2	1446.3	1414.3	707.1	3.68	0.033
PS	2	194.6	115.6	57.8	0.30	0.742
NC	2	438.5	439.5	219.8	1.14	0.328
LT×PS	4	635.2	725.5	181.4	0.94	0.448
LT×NC	4	702.5	698.4	174.6	0.91	0.467
PS×NC	4	412.1	379.9	95.0	0.49	0.740
LT×,PS×NC	8	713.4	713.4	89.2	0.46	0.875
Error	45	8652.6	8652.6	192.3		
Total	71	13,195.2				

Analysis of variance for flatness of horizontal surfaces P

$FLAT_P$), their combinations have been analyzed as well. The degrees of freedom, the sum of squares, the adjusted sum of squares, and the adjusted mean squares of the correspondent source are described by DOF, Seq SS, Adj SS, and Adj MS columns, respectively. The results in the *F* column are calculated by dividing the adjusted mean squares of the source by the adjusted mean square of the error and are of fundamental importance for verifying or rejecting the test statistics hypothesis that the source significantly affects the response ($FLAT_P$). When *F* is higher than the related percentile of *F*-distribution, evaluable by the DOF of the source and the total number of DOF, the considered source affects the response while, on the contrary, if *F* is lower than the *F*-distribution percentile, the source influence is negligible. The last column of the ANOVA table presents the value of the parameter *p*, which is a more convenient indicator for the assessment of the source influence. The value of *p* is automatically calculated by the statistic software employed for the analysis as a function of *F*, the related *F*-distribution percentile, DOF of the source, and DOF of the Error. Depending on the selected CI, 95% in the present work, when *p* results to be higher than 1 – CI, meaning 0.05, the assumption of the null hypothesis H_0 is correct, indicating in practice that the source has not significant influence

Fig. 7 Main effects plot for $FLAT_P$

Fig. 8 Probability plot of $FLAT_S$ (in μm) resulting from normality test

4.1.2 Flatness of vertical surfaces
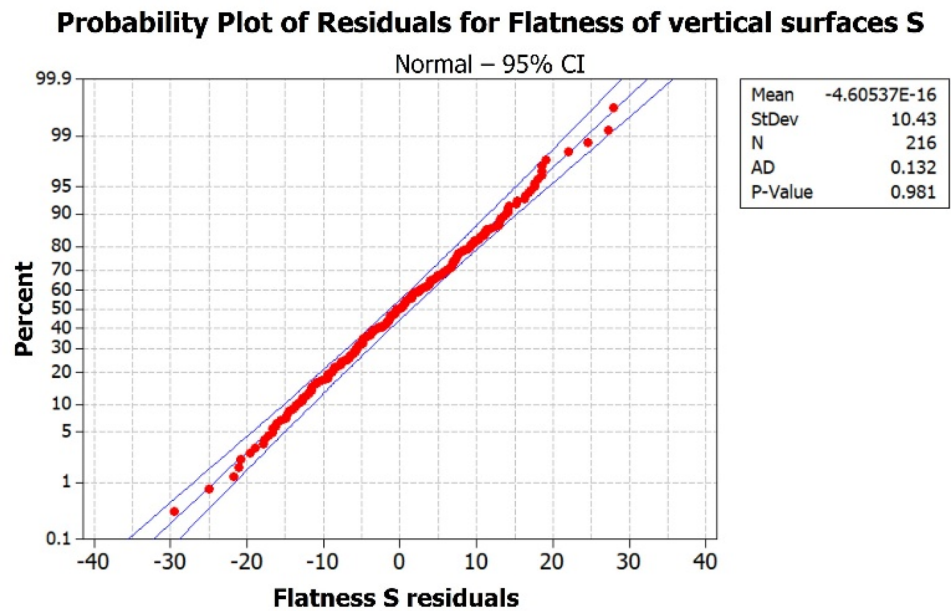
on the response. On the other hand, if the *p* value is lower than 0.05, the alternative hypothesis H_1 has to be considered correct, which indicates a significant effect of the source.

Based on the results of the analysis in Table 7, it can be noticed that the only parameter affecting the flatness of the printed horizontal surfaces is the *LT* ($p = 0.033$). More in details, by observing the main effects plot of Fig. 7, the flatness tends to grow as *LT* increases, even by considering the presence of a maximum of $FLAT_P$ for intermediate values of *LT*, leading to a worsening of the final geometric accuracy of the component. The near constancy of *PS* effect plot and the slope of *NC* lower than *LT* underline again the lack of influence of *NC* and *PS* on horizontal surface flatness, even though a general increase of $FLAT_P$, when increasing both *NC* and *PS*, is detectable.

The analysis procedure has been repeated consistently for the other dependent variables.

The results of the measurements of the flatness of vertical surfaces $FLAT_S$ are reported in Appendix Table 22. The normality test of the related data is shown in the probability plot of Fig. 8, where the verification of the normality assumption is clearly visible. All the acquired data are correctly bounded by the two CI curves.

The analysis of variance for $FLAT_S$ (Table 8) underlines that the *LT* and the *NC* affect the flatness of the printed vertical surfaces, while *PS* and all the interactions between the process parameters do not affect it. The examination of the main effects plot (Fig. 9), where the contribution of *LT* presents a positive slope, the evolution of *NC* shows a negative slope, and the graph of *PS* is practically horizontal, confirms the previous assessment. In particular, an increase of the *LT* worsens the vertical flatness, as expected by the previously

Table 8 ANOVA for $FLAT_S$

Analysis of variance for flatness of vertical surfaces S						
Source	DOF	Seq SS	Adj SS	Adj MS	*F*	*p*
LT	2	5693.2	5693.2	2846.6	22.99	< 0.001
PS	2	616.2	616.2	308.1	2.49	0.086
NC	2	144,285.5	144,285.5	72,142.8	582.70	< 0.001
LT×PS	4	423.8	423.8	106.0	0.86	0.492
LT×NC	4	773.4	773.4	193.4	1.56	0.186
PS×NC	4	611.8	611.8	152.9	1.24	0.297
LT×PS×NC	8	1586.2	1586.2	198.3	1.60	0.127
Error	189	23,399.9	23,399.9	123.8		
Total	215	177,390.0				

Main Effects Plot for Flatness of vertical surfaces S
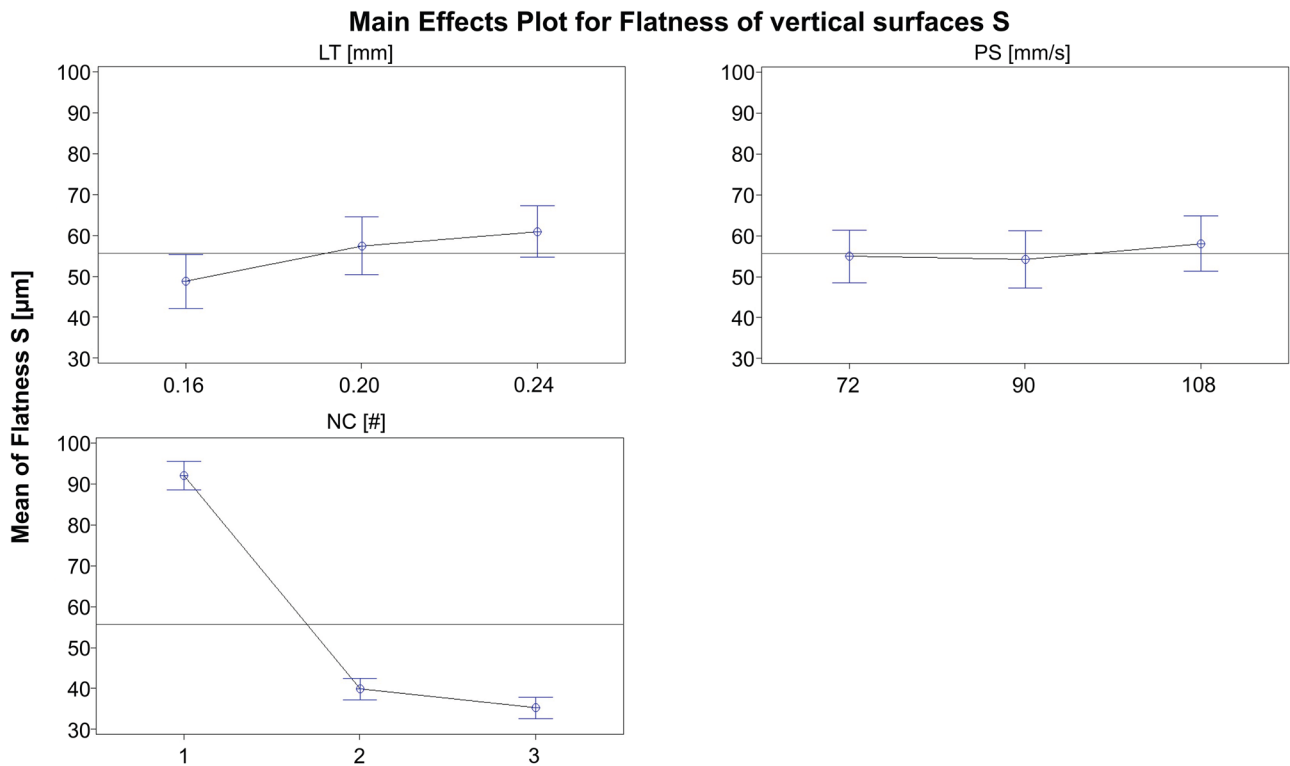

Fig. 9 Main effects plot for $FLAT_S$

reported bibliographic analysis (Table 1), in which the increase of *LT* reduces the accuracy of the deposited layer, which consequently negatively affects flatness as well. The increment of *NC*, instead, yields the structure of the part more robust, enhancing the stability of the deposition of the successive layers, positively influencing $FLAT_S$.

4.1.3 Flatness of inclined surfaces

Appendix Table 23 shows the measurements of flatness of inclined surfaces $FLAT_I$. The normality test has been performed, revealing a lack of normality in the data. Consequently, an ANOVA has been performed permitting to

Fig. 10 Probability plot of $FLAT_I$ (in μm) resulting from normality test
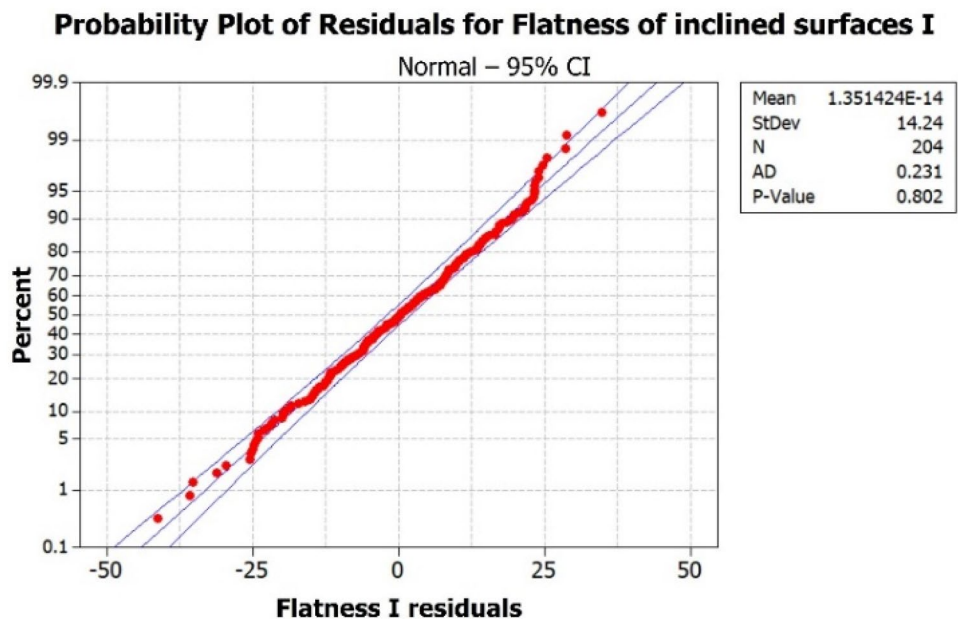
Table 9 ANOVA for $FLAT_I$

Source	DOF	Seq SS	Adj SS	Adj MS	F	p
			Analysis of variance for flatness of inclined surfaces I			
LT	2	4939.3	6490.3	3245.1	13.95	<0.001
PS	2	1808.4	1911.6	955.8	4.11	0.018
NC	2	69,367.2	69,789.5	34,894.8	149.98	<0.001
LT×PS	4	456.7	389.7	97.4	0.42	0.795
LT×NC	4	2833.4	2774.2	693.5	2.98	0.021
PS×NC	4	825.4	791.6	197.9	0.85	0.495
LT×PS×NC	8	2816.8	2816.8	352.1	1.51	0.155
Error	177	41,181	41,181	232.7		
Total	203	124,228.1				

identify and eliminate possible outliers. The probability plot of the set of data without the found outliers is depicted in Fig. 10 and exhibits that the normality assumption is verified.

The results of the ANOVA (Table 9) indicate that the single effects of all the three parameters influence the response $FLAT_I$. The interaction between the LT and NC affects it too. The main impacts on the response are those related to LT and NC, as suggested by the lower values of the parameters p, while PS and the LT interaction with NC have a limited effect. This is inferable from the higher slopes of LT and NC in the main effects plot of Fig. 11 as well. Increasing both LT and PS results in an increase of $FLAT_I$ due to, also

in this case, the reduction of the precision of the deposition technique underlined by other studies reported in Table 1. Once again, incrementing the NC improves the stability of the FDM process, giving rise to a reduction of $FLAT_I$.

The results show that, on average, the $FLAT_I$ is more than 15% larger than $FLAT_S$ and $FLAT_P$, which, in turn, have comparable values. This result highlights the usefulness of having devised a geometry to measure surfaces that are oriented differently. In addition, this difference can be explained through the staircase effect, which is more pronounced in inclined surfaces. Indeed, in horizontal surfaces, the staircase effect is practically absent. In vertical surfaces,
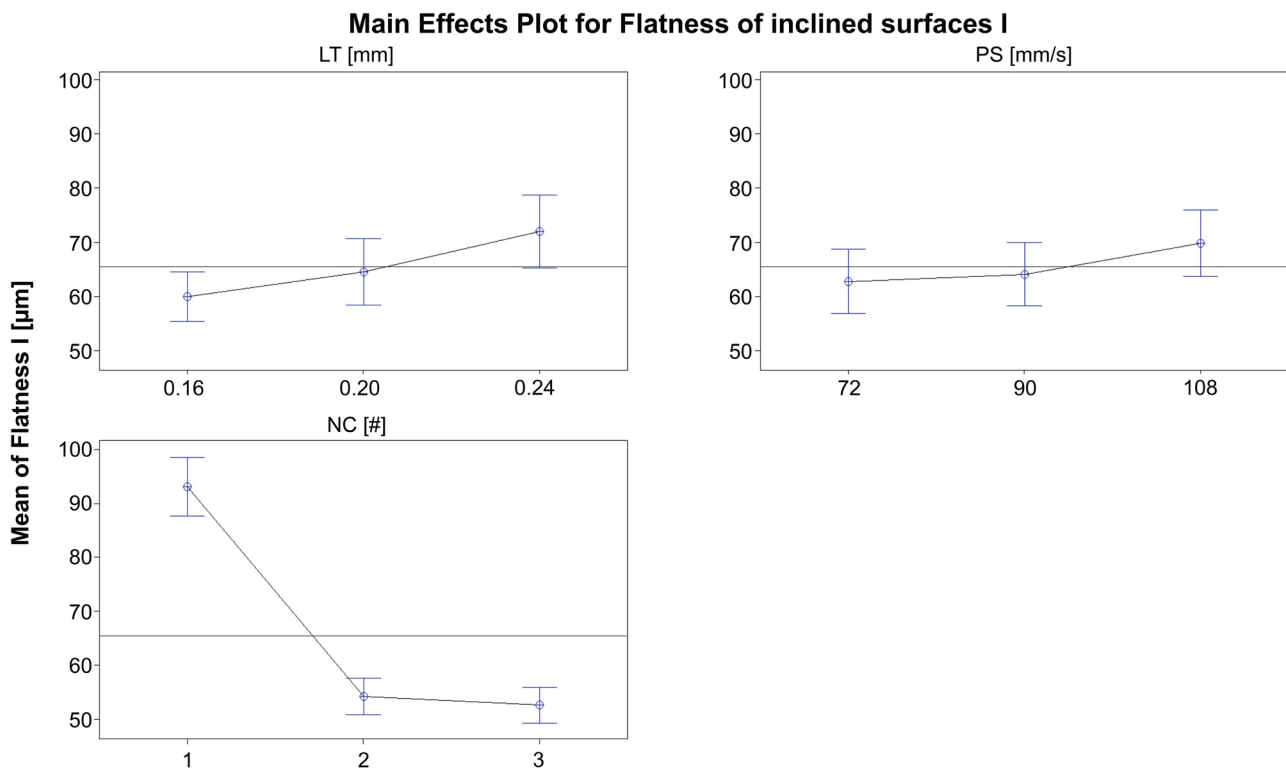
Fig. 11 Main effects plot for $FLAT_I$

Fig. 12 Probability plot of CYL_C (in μm) resulting from normality test
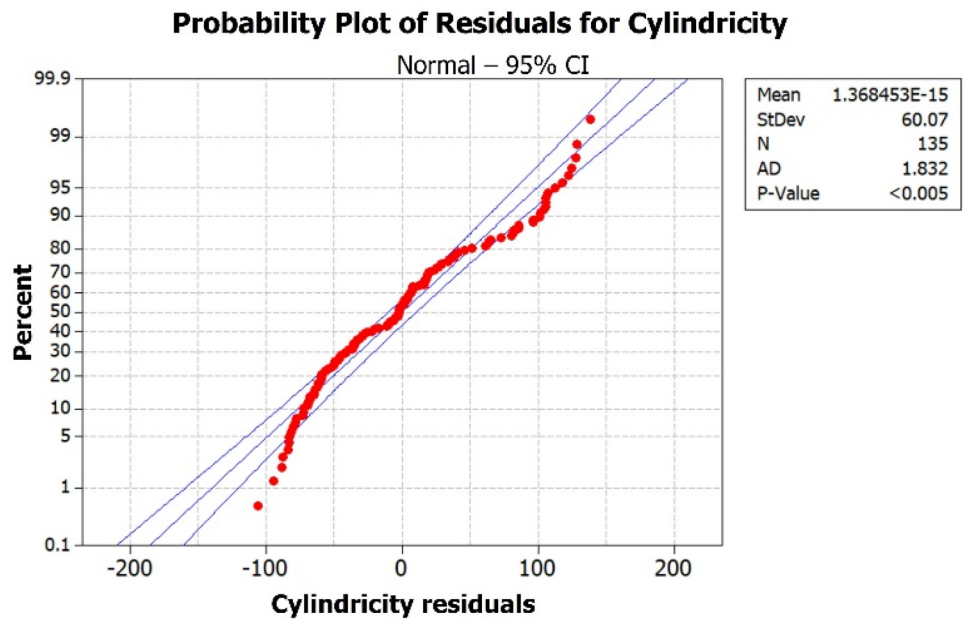
the staircase effect is difficult to identify with the CMM touch probe because the sphere cannot reach the valleys of the slices. On the other hand, as for inclined surfaces, the valleys are more easily reached by the touch probe sphere and the $FLAT_I$ can be consequently affected. The geometric deviations of inclined surfaces can also be affected (compared with vertical or horizontal surfaces) by a smaller support area of the different skin layers.
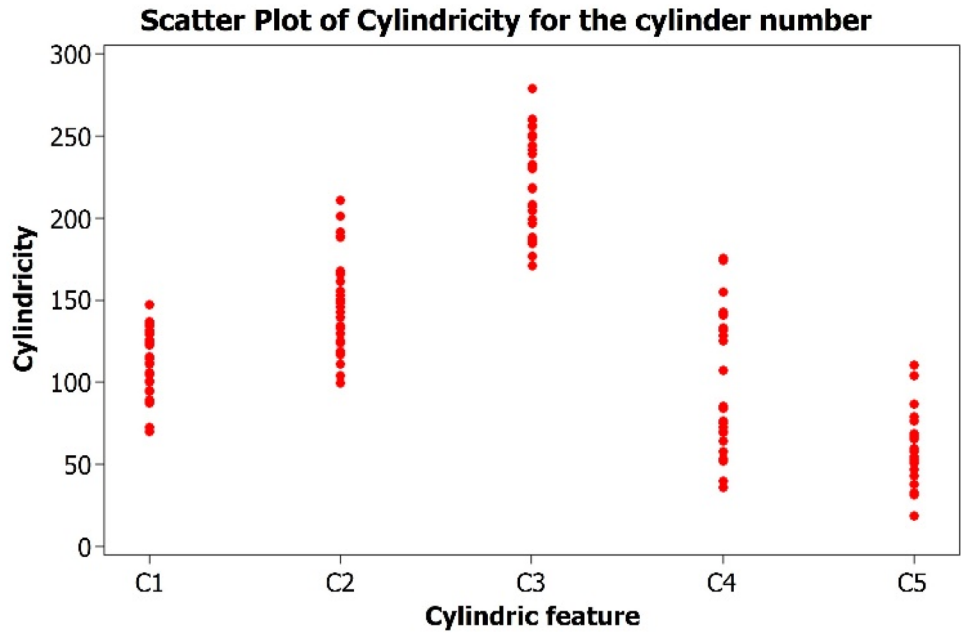
4.1.4 Cylindricity

The measurements of cylindricity deviations of all the features, vertical and inclined ones, are summarized in Appendix Table 24. Figure 12 and Table 10 show the results of the related normality test and of the preliminary ANOVA, respectively.

The lack of normality and the total independence of CYL_C from the process parameters are clearly understandable. In this case, since the standardized residual values of the data external to the CI boundaries are lower than 3 times the standard deviation, they cannot be considered as outliers and cannot be removed from the analysis. Moreover, the fact that CYL_C is completely independent from the sources is suspicious. In order to better investigate this situation, a scatter plot of cylindricities data, a graphical representation of them by groups, in which each group represents a determined cylindricity feature, has been obtained (Fig. 13). From the distribution of the data in the scatter plot, a good distinction between the vertical cylindricities, namely CYL_{C1}, CYL_{C2}, and CYL_{C3}, and the inclined ones, CYL_{C4}, and CYL_{C5}, is detectable. Due to this, it is not possible to consider the analysis as 5 repetitions of the 27 tests, but it has to be subdivided into two different analyses: the first one

Table 10 ANOVA for CYL_C

Analysis of variance for cylindricity of all holes C1–C5						
Source	DOF	Seq SS	Adj SS	Adj MS	F	p
LT	2	2103	2103	1051	0.23	0.791
PS	2	24,579	24,579	12,289	2.74	0.069
NC	2	5869	5869	2934	0.66	0.521
$LT \times PS$	4	2280	2280	570	0.13	0.972
$LT \times NC$	4	281	281	70	0.02	1.000
$PS \times NC$	4	2994	2994	748	0.17	0.955
$LT \times PS \times NC$	8	1015	1015	127	0.03	1.000
Error	108	483,570	483,570	4478		
Total	134	522,691				

Fig. 13 Scatter plot of cylindricity by groups

concerning the vertical features, consisting of 27 tests with 3 repetitions, and the second one associated to the inclined features, involving 27 tests with 2 repetitions.

The normality assumption for the data related to the cylindricity of vertical features CYL_{Cv} is verified, as observable in Fig. 14. The ANOVA of CYL_{Cv} (Table 11) and the main effects plot of Fig. 15 indicate that this geometric deviation is negatively affected by PS while positively influenced by NC. The reason of these behaviors is still ascribable to the reduction of precision due to an increased deposition speed, and to the enhancement of stability with a higher NC.

Figure 16 illustrates that the normality assumption for the data of the cylindricity of the inclined holes CYL_{Ci} is confirmed.

The ANOVA of CYL_{Ci} demonstrates that, as for CYL_{Cv}, the cylindricity of the inclined holes are significantly influenced by PS and NC (Table 12).

Refining the analysis by the evaluation of the main effects plot for CYL_{Ci} of Fig. 17, the negative effect of a PS increase can be assessed. The p value of the PS influence in Table 12 is lower than the one calculated in Table 11. Thus, the effect of PS is more prominent on the cylindricity

Fig. 14 Probability plot of CYL_{Cv} (in μm) resulting from normality test
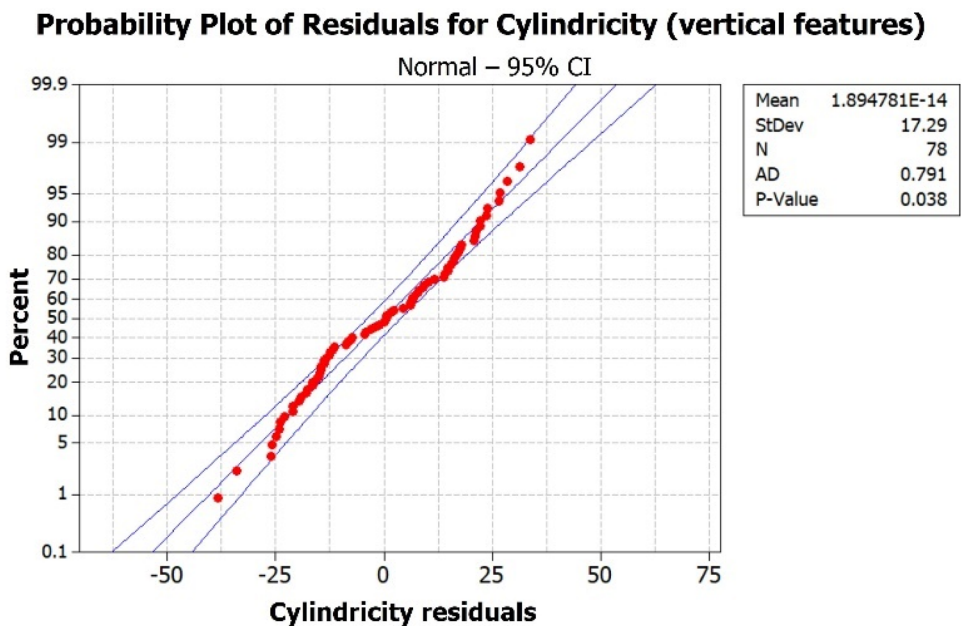
Table 11 ANOVA for CYL_{Cv}

| Analysis of variance for cylindricity of vertical features C1–C3						
Source	DOF	Seq SS	Adj SS	Adj MS	F	p
LT	2	684.5	896.6	448.3	0.95	0.392
PS	2	6259.6	6200.8	3100.4	6.60	0.003
NC	2	13,455.5	13,738.4	6869.2	14.63	<0.001
LT×PS	4	1641.6	1435.0	358.8	0.76	0.554
LT×NC	4	215.4	255.5	63.9	0.14	0.968
PS×NC	4	2078.2	1994.7	498.7	1.06	0.385
LT×PS×NC	8	1850.9	1850.9	231.4	0.49	0.855
Error	51	23,007.1	23,007.1	469.5		
Total	77	215,110.2				

of the inclined holes with respect to the vertical ones. This can be explained by considering that, in the case of inclined holes, a cantilever effect takes place between two subsequent deposited layers. An increase of the *PS* led to a shorter cooling time of the layer that, being subjected to its own weight, and having a lower mechanical resistance, results to be less stable, decreasing the feature precision. Moreover, even if the *LT* does not significantly affect CYL_{Ci}, the cantilever effect is increased when *LT* is greater, as visible by the positive slope of *LT* curve in Fig. 17. The contribution of *NC* to CYL_{Ci} shows to have an optimum condition for the intermediate value of 2, while the highest value worsens

the cylindricity quality. This behavior cannot be explained at present and should be further investigated.

4.1.5 Concentricity

The data related to the measurements of concentricity between the different cylindrical features (Appendix Table 25) complies with the normality assumption (Fig. 18). $CONC_{CxCy}$ is greatly influenced by *LT* and *PS*, as highlighted by the ANOVA analysis of Table 13. The positive slopes of the curves in the main effects plot (Fig. 19) reveal that both the influencing process parameters have negative effects on the
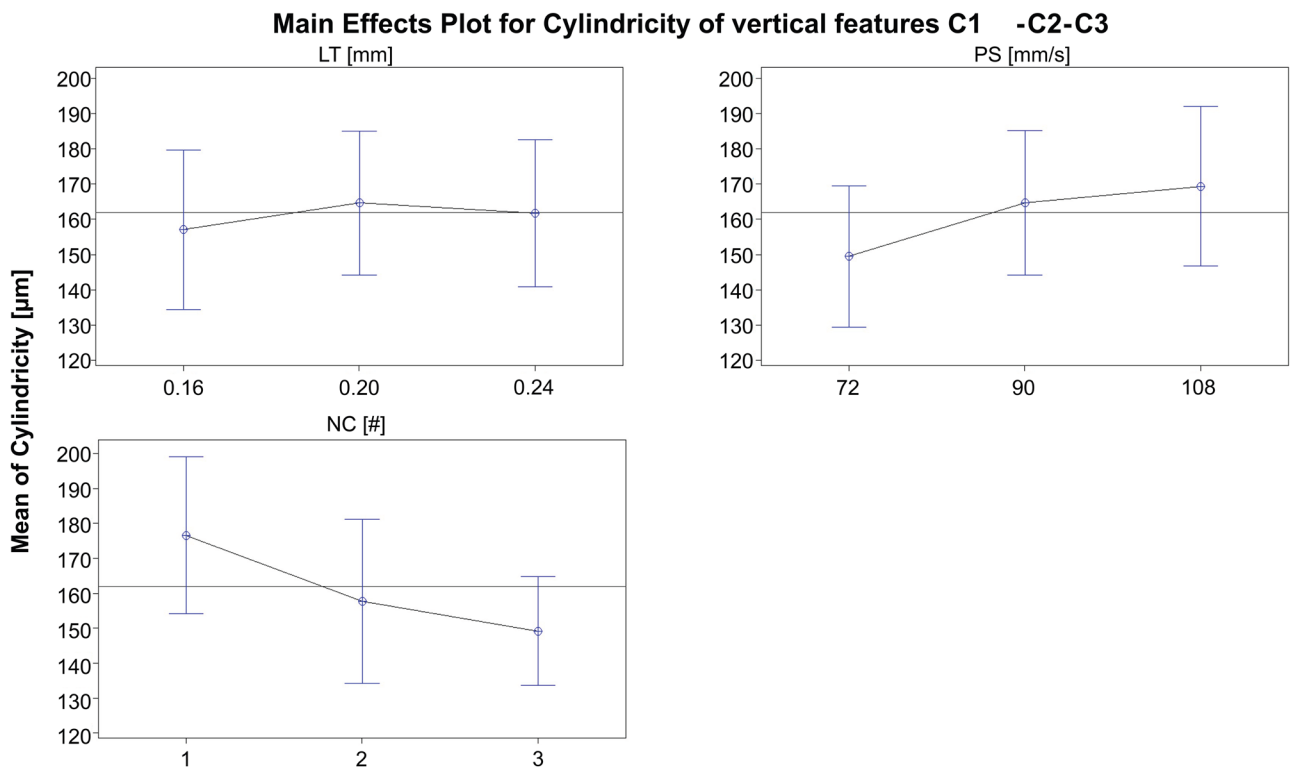
Fig. 15 Main effects plot for CYL_{Cv}

Fig. 16 Probability plot of CYL_{Ci} (in µm) resulting from normality test
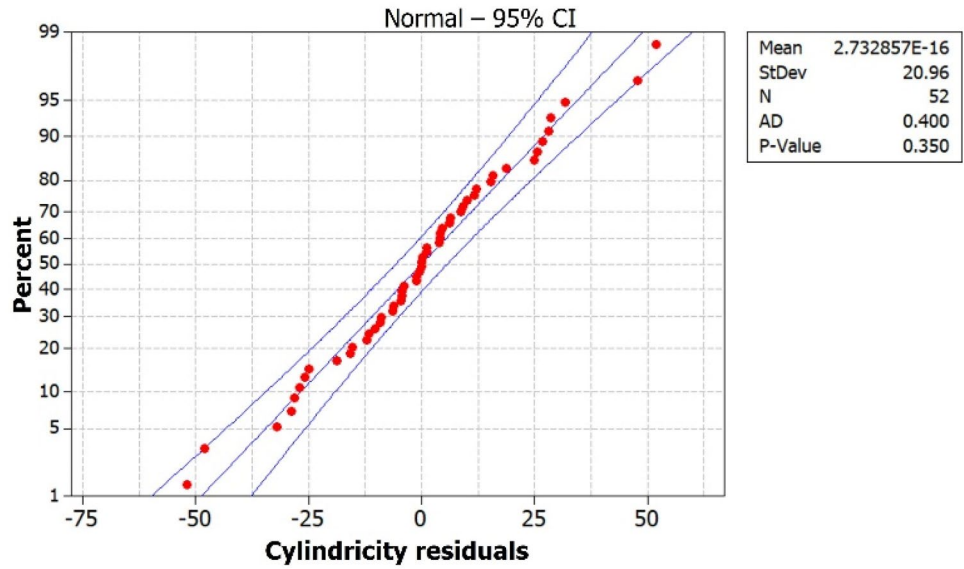
response. Once again, the growth of *LT* and *PS* causes an accuracy diminishment of the FDM process.

4.1.6 Surface parallelism for horizontal surfaces

Figures 20 and 21 and Table 14 report the probability plot, the main effects plot, and the ANOVA results for the parallelism between the horizontal surfaces PAR_{PxPy} (Appendix Table 26), respectively.

Since the normality assumption of the data is verified, the ANOVA results, revealing a significant influence of *LT* and *NC* on PAR_{PxPy}, can be considered reliable. Figure 21 indicates that increasing the influencing parameters, the parallelism of horizontal surfaces rises as well. This behavior has been already observed for $FLAT_P$ and is due to the correlation between the two horizontal features. The medians of PAR_{PxPy} as a function of *LT* and *NC* show a maximum for the intermediate values of these latter (*LT* = 0.20 mm, *NC* = 2), which indicate a non-monotone evolution. In these positions, anyway, the dispersion of the acquired data

is high, as visible by the large measure intervals; thus, the true median could result lower than represented, leading to a monotone function of parallelism, and indicating a general worsening of the parallelism when *LT* and *NC* increase.

4.1.7 Surface parallelism for vertical surfaces

The probability plot of the data (Appendix Table 27) of parallelism between vertical surfaces (Fig. 22) exhibits normality.

Looking at the related ANOVA results (Table 15), all the effects of the single process parameters are significant, while their interactions do not affect PAR_{SxSy}.

Among the process parameters, the most influencing one is *NC*, as suggested by the lowest value of *p* and the highest slope of the main effect plot curve (Fig. 23). Because of the deposition precision reduction when increasing both *LT* and *PS*, these latter negatively affect the vertical surface parallelism, while the increased robustness induced by an augmented *NC* has a positive effect on it.

Table 12 ANOVA for CYL_{Ci}

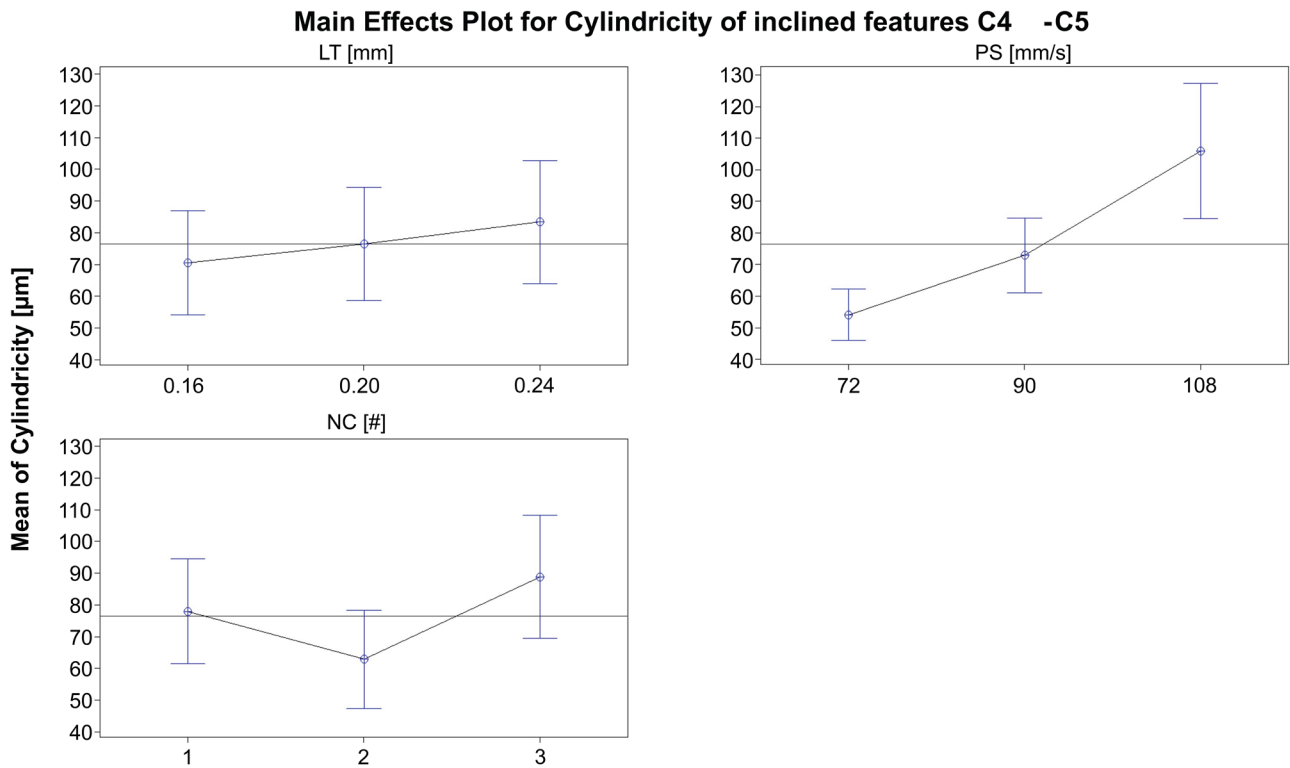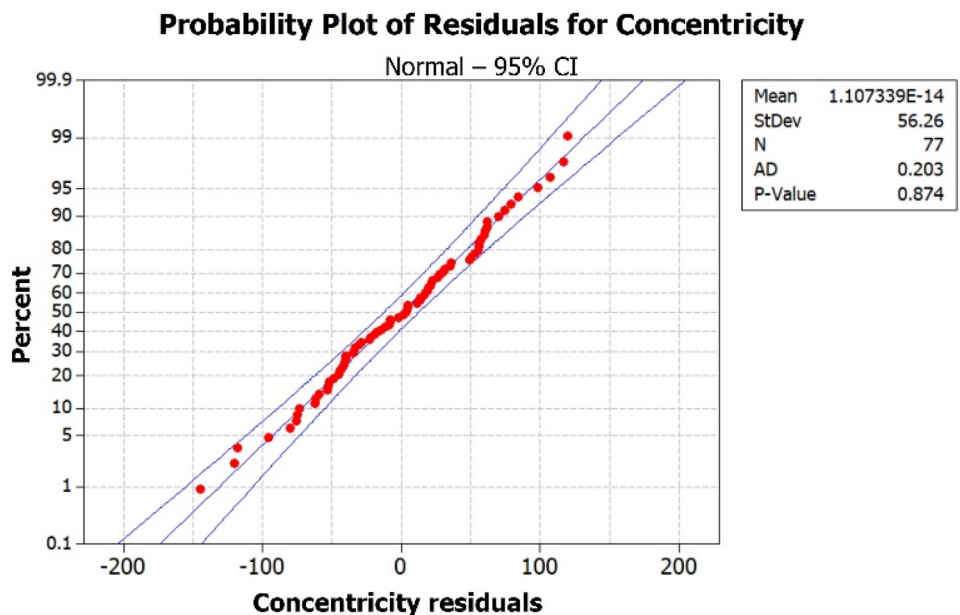| Analysis of variance for cylindricity of inclined features C4–C5						
Source	DOF	Seq SS	Adj SS	Adj MS	*F*	*p*
LT	2	1381.7	2499.2	1249.6	1.39	0.267
PS	2	24,107.9	23,997.7	11,998.9	13.39	<0.001
NC	2	5764.5	7305.9	3653.0	4.08	0.029
LT×*PS*	4	766.8	682.7	170.7	0.19	0.941
LT×*NC*	4	1272.0	2076.1	519.0	0.58	0.680
PS×*NC*	4	2934.4	3248.4	812.1	0.91	0.475
LT×*PS*×*NC*	8	2987.5	2987.5	373.4	0.42	0.900
Error	25	22,401.6	22,401.6	896.1		
Total	51	61,616.5				

Fig. 17 Main effects plot for CYL_{Ci}

4.1.8 Surface perpendicularity

The normality test for the perpendicularity of vertical surfaces S with respect to the horizontal surface P1 has been passed, as reported in the plot of Fig. 24. The related experimental measurements are reported in Appendix Table 28.

From the ANOVA results (Table 16), the dependency of $PERP_{SxP1}$ from all the single effects of the process parameters is detectable. Also in this case, LT and PS negatively affect the response, while this is positively influenced by the increased stability deriving from a high NC (Fig. 25).

Fig. 18 Probability plot of $CONC_{CxCy}$ (in μm) resulting from normality test

Table 13 ANOVA for $CONC_{CxCy}$

Analysis of variance for concentricity of vertical holes C1–C3							
Source	DOF	Seq SS	Adj SS	Adj MS	F	p	
LT	2	70,065	66,613	33,306	6.92	0.002	
PS	2	124,699	121,132	60,566	12.59	<0.001	
NC	2	25,183	25,356	12,678	2.64	0.082	
LT×PS	4	43,751	41,325	10,331	2.15	0.089	
LT×NC	4	2151	2130	533	0.11	0.978	
PS×NC	4	9756	8892	2223	0.46	0.763	
LT×PS×NC	8	23,371	23,371	2921	0.61	0.767	
Error	50	240,520	240,520	4810			
Total	76	539,496					

4.2 Regression analysis

Starting from the ANOVAs of the considered responses, the process parameters mainly affecting them have been identified. With the intent of developing a set of mathematical models to forecast the geometric deviations as a function of the affecting parameters, a regression analysis for each response has been performed. This led to the Eqs. from (1) to (9):

$$FLAT_P = 18.3 + 105 \cdot LT \tag{1}$$

$$FLAT_S = 81.7 + 150.4 \cdot LT - 28.2 \cdot NC \tag{2}$$

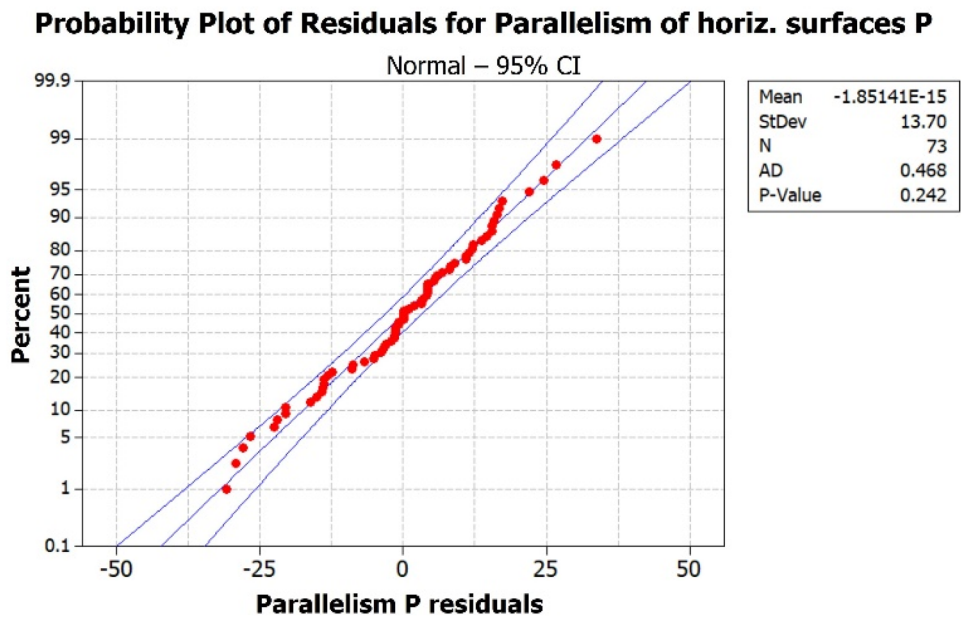$$FLAT_I = 7.6 + 402.2 \cdot LT + 0.2 \cdot PS + 3.5 \cdot NC - 117.7 \cdot LT \cdot NC \tag{3}$$

$$CYL_{Cv} = 136.9 + 0.6 \cdot PS - 14.7 \cdot NC \tag{4}$$

$$CYL_{Ci} = -64.4 + 1.4 \cdot PS + 6.1 \cdot NC \tag{5}$$

$$CONC_{CxCy} = -144.3 + 908.0 \cdot LT + 2.7 \cdot PS \tag{6}$$

Main Effects Plot for Concentricity
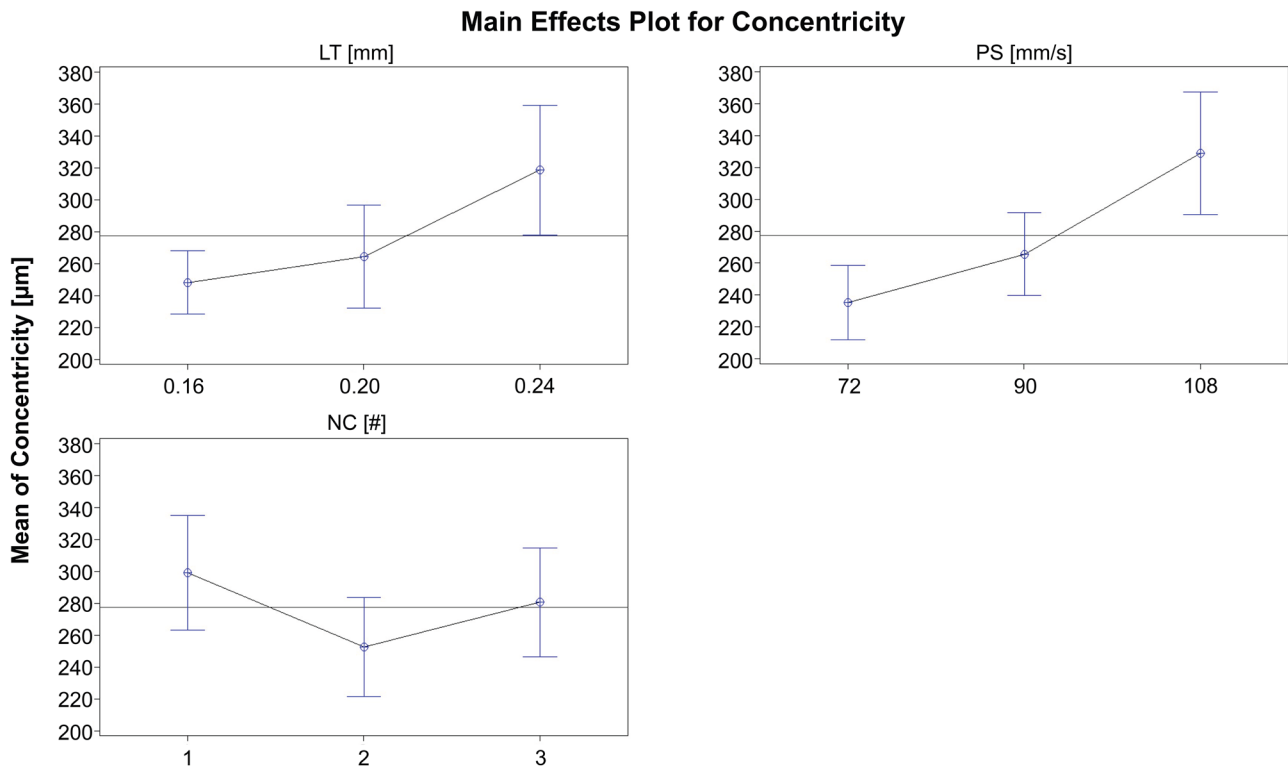
Fig. 19 Main effects plot for $CONC_{CxCy}$

Probability Plot of Residuals for Parallelism of horiz. surfaces P

Normal – 95% CI

Mean	-1.85141E-15
StDev	13.70
N	73
AD	0.468
P-Value	0.242

$$PAR_{PxPy} = 57.4 + 1.6 \cdot LT - 19.7 \cdot NC + 123.4 \cdot LT \cdot NC \quad (7)$$

$$PAR_{SxSy} = 54.2 + 227.0 \cdot LT + 0.4 \cdot PS - 20.6 \cdot NC \quad (8)$$

$$PERP_{SxP1} = 69.0 + 178.7 \cdot LT + 0.2 \cdot PS - 28.6 \cdot NC \quad (9)$$

For assessing the capability of the introduced mathematical models to correctly estimate the related geometric deviations, they were applied for calculating these latter by considering the combination of *LT*, *PS*, and *NC* and comparing the model outcomes with the experimental ones. Table 17 reports the minimum (e_{min}), maximum (e_{MAX}), and
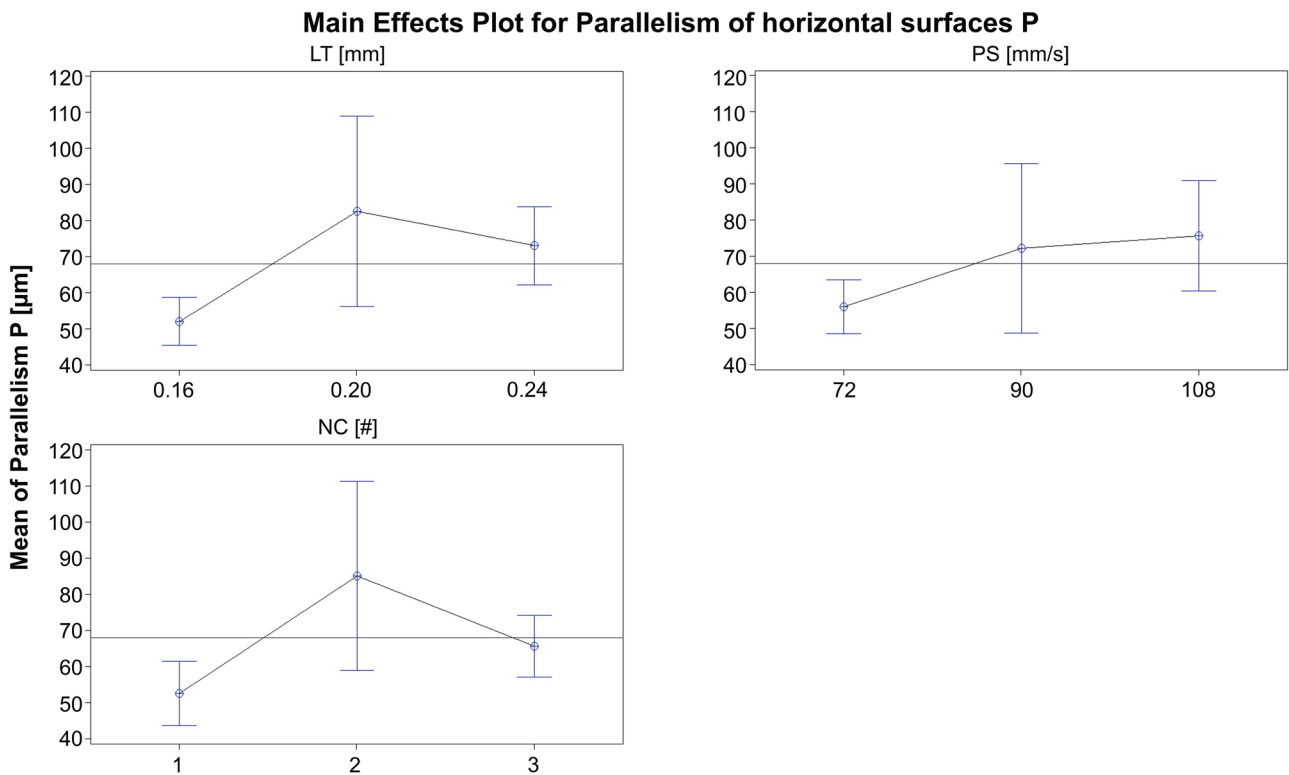
Fig. 21 Main effects plot for PAR_{PxPy}

Table 14 ANOVA for PAR_{PxPy}

Analysis of variance for parallelism between horizontal surfaces P

Source	DOF	Seq SS	Adj SS	Adj MS	F	p
LT	2	10,945	7630	3815	3.79	0.030
PS	2	4070	3437	1719	1.71	0.192
NC	2	9773	8288	4144	4.12	0.023
LT×PS	4	6740	7476	1869	1.86	0.134
LT×NC	4	22,382	14,182	3546	3.52	0.014
PS×NC	4	1838	2558	640	0.64	0.640
LT×PS×NC	8	12,285	12,285	1536	1.53	0.174
Error	46	46,273	46,273	1006		
Total	72	114,304				

percentage ($e_{\%}$) errors resulting from this comparison. For each geometric feature and process parameters' combination, the difference between measured and modelled data was calculated. Among these, e_{min} and e_{MAX} represent the minimum and the maximum values achieved, respectively. The average of the single percentage errors deriving from the calculated differences was defined as $e_{\%}$.

Despite the presence of a low $e_{\%}$ for geometric features such as $FLAT_I$, CYL_{Cv}, and $CONC_{CxCy}$, the calculation errors for $FLAT_S$ and PAR_{PxPy} are above 20%, resulting in an average percentage error of 15%. Even if greater errors in $FLAT_S$ and PAR_{PxPy} estimation can be made with respect to the evaluation of the other geometric deviations, this average value is still good, indicating a general good prediction ability of the mathematical models. In this manner, an indication of the final part geometric characteristics, once the process parameters have been selected, can be achieved. The process parameters optimization can be accomplished as a function of the desired

geometric characteristics. The occurrence of high $e_{\%}$ values for some responses is ascribable to the fact that, as observed in Table 1, several process parameters affect the printed part quality. In addition to LT, PS, and NC, other parameters, such as raster-to-air gap, infill density, nozzle temperature, have a significant influence on the geometric deviations. Since the proposed models concern only the variation of the process parameters reported in Table 4, it is not possible to consider the effects of other parameters. Hence, to improve the models' performances, further experiments foreseeing different printing parameters should be performed.

4.3 Printing times

The *PTs*, expressed in minutes for all the performed tests, are reported in Table 5. The values satisfy the normality assumption (Fig. 26).

Fig. 22 Probability plot of PAR_{SxSy} (in μm) resulting from normality test

Table 15 ANOVA for PAR_{SxSy}

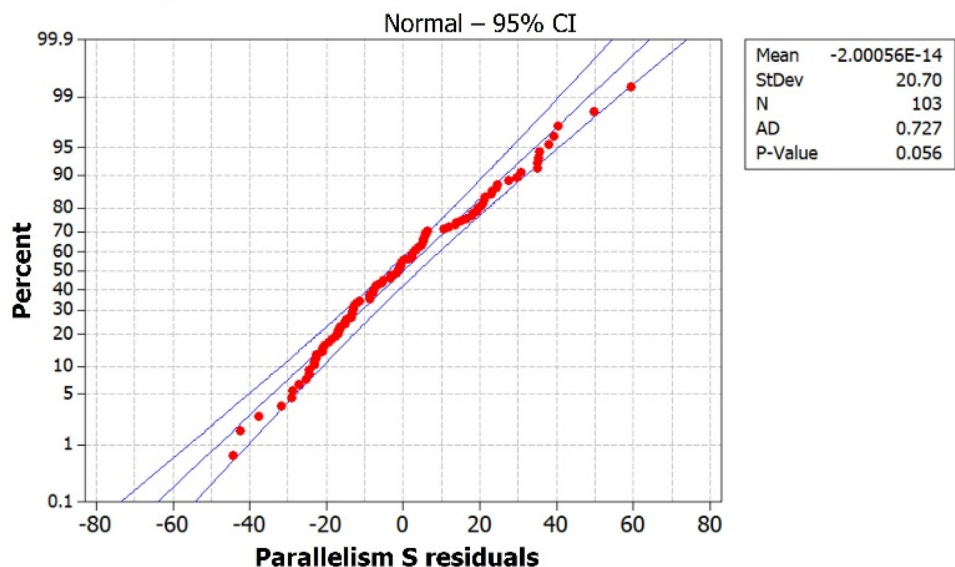| Analysis of variance for parallelism between vertical surfaces S						
Source	DOF	Seq SS	Adj SS	Adj MS	F	p
LT	2	9131.2	8883.0	4441.5	7.73	0.001
PS	2	5151.6	5059.4	2529.7	4.40	0.016
NC	2	44,484.9	41,639.3	20,819.7	36.21	<0.001
LT×PS	4	2306.0	2030.0	507.5	0.88	0.478
LT×NC	4	2630.4	3106.4	776.6	1.35	0.259
PS×NC	4	2086.5	2357.4	589.4	1.03	0.400
LT×PS×NC	8	878.2	878.2	109.8	0.19	0.991
Error	76	43,694.7	43,694.7	574.9		
Total	102	110,363.5				

As expected, the ANOVA (Table 18) indicates that all the process parameters significantly affect the production time. Particularly, when increasing the *LT* and the *PS*, the time needed for the realization of the part is reduced, while if the *NC* is increased, the FDM process requires more time (Fig. 27).

The regression analysis of the data permitted to derive the regression equation able to calculate the *PT* as a function of the process parameters (Eq. (10)).

$$PT = 366 - 679 \cdot LT - 1.26 \cdot PS + 13.4 \cdot NC \qquad (10)$$

The comparison of the *PTs* calculated by Eq. (10) and the experimental ones (Table 19), gives a mean of the percentage error of 2.87%, a maximum error of 12.03%, and a minimum error of 0.05%. The values of the error can be considered acceptable, which underline the goodness of the regression model.

4.4 Effects of parameters on quality vs. printing time

Tables 17 and 19, which summarize the calculation errors by applying the derived regression models in Eqs. (1–10), confirm their reliability in the estimation of the geometric deviations and the *PTs* as a function of the employed range

Main Effects Plot for Parallelism of vertical surfaces S
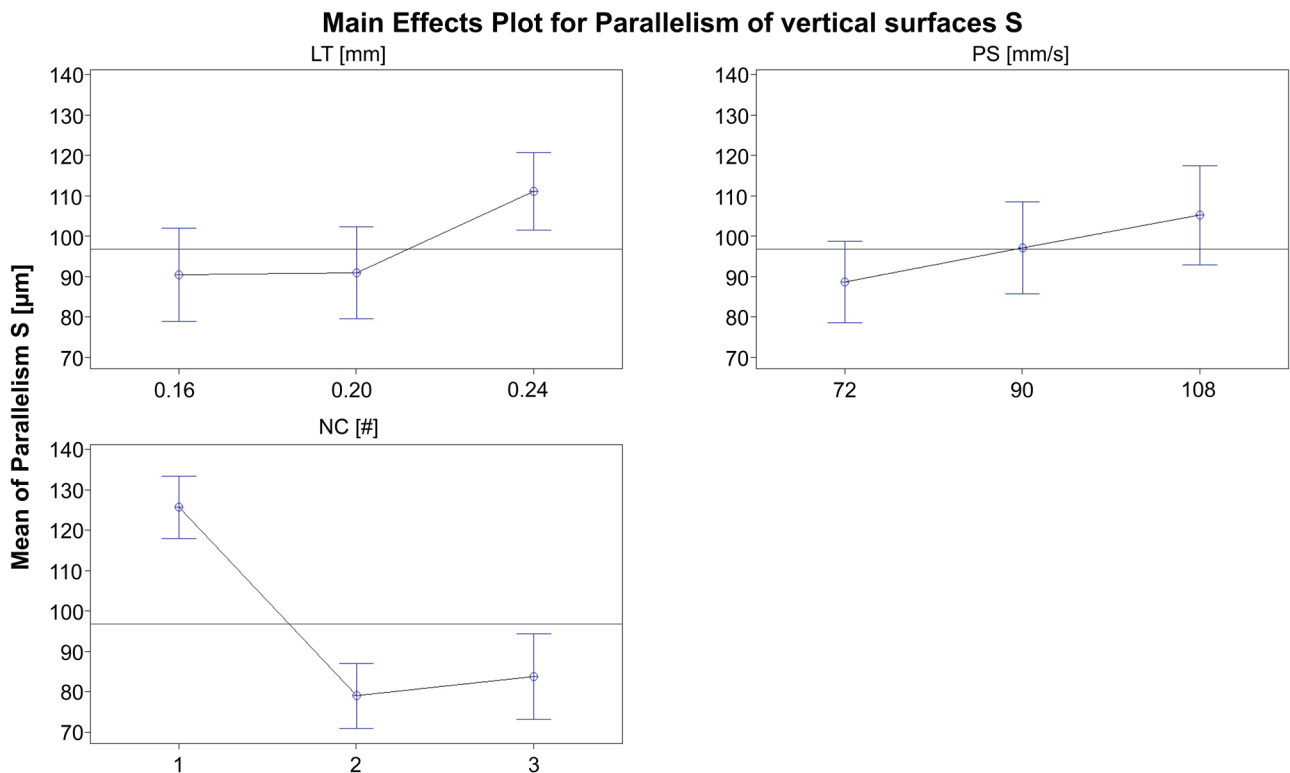
Fig. 23 Main effects plot for PAR_{SxSy}

Probability Plot of Residuals for Perpend. of vert. surf. S to P1

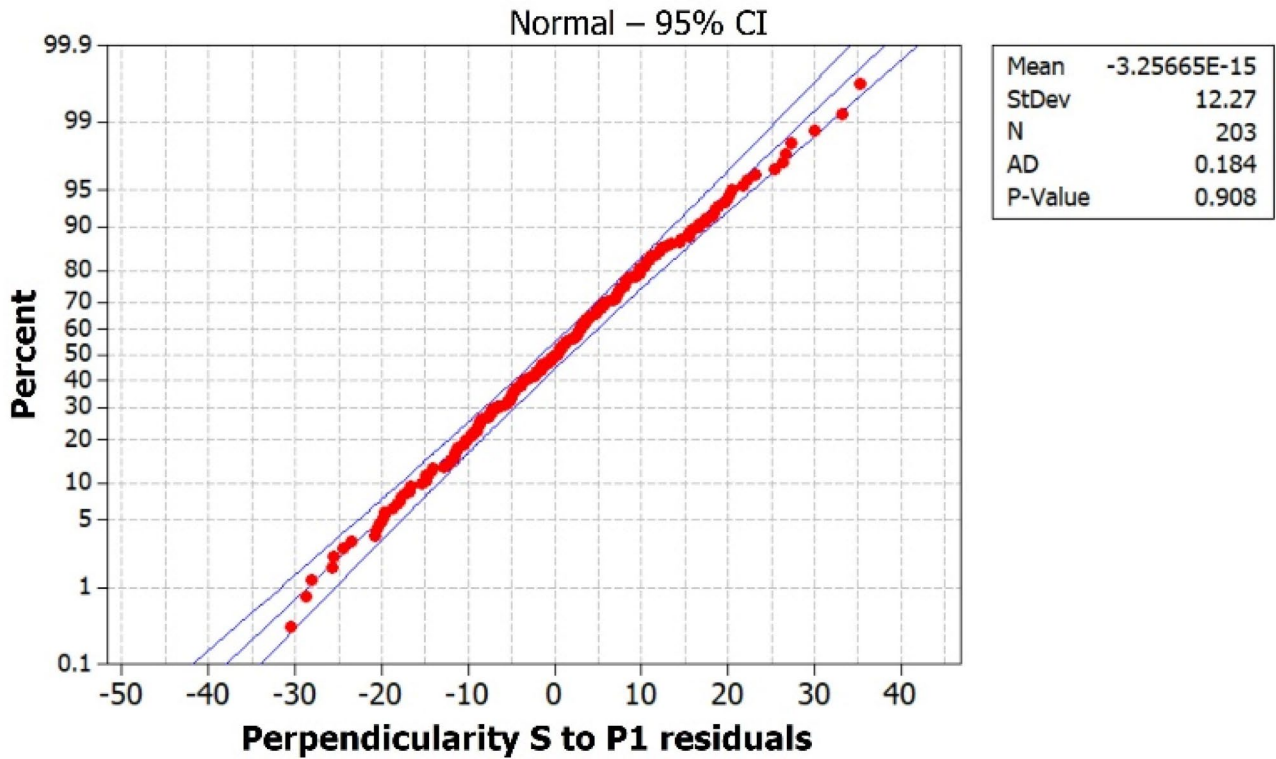**Fig. 24** Probability plot of $PERP_{SxP1}$ (in μm) resulting from normality test

of the process parameters. Therefore, the proposed models can be further analyzed for optimization scopes in compliance with the objectives stated in Sect. 1.

Figure 28 shows the evolution of the estimated geometric deviations as a function of the PT. As expected, the tendency of a general enhancement of the quality, meaning a reduction of the geometric deviations, when the PT increases, is clearly visible. As previously observed, this is due to the lowering of LT and PS, and to the increase of NC, that improves the

FDM deposition process while at the same time increasing the PT (Fig. 27). Consequently, in order to minimize geometric deviations, a higher PT is unsurprisingly required.

To better understand how the process parameters affect the PT and the totality of the geometric deviations, their values have been normalized and represented as a percentage of their amounts. More in detail, the normalization of the employed process parameters has been performed by applying Eq. (11):

Table 16 ANOVA for $PERP_{SxP1}$

Analysis of variance for perpendicularity between vertical surfaces and P1

Source	DOF	Seq SS	Adj SS	Adj MS	F	p
LT	2	7857.5	7972.2	3986.1	30.97	< 0.001
PS	2	1575.8	2023.5	1011.8	7.86	0.001
NC	2	129,610	125,435	62,717.5	487.34	< 0.001
$LT \times PS$	4	574	705.3	176.3	1.37	0.246
$LT \times NC$	4	1077.5	1207.4	301.8	2.35	0.056
$PS \times NC$	4	860.4	882.1	220.5	1.71	0.149
$LT \times PS \times NC$	8	1649.7	1649.7	206.2	1.60	0.127
Error	176	22,650.2	22,650.2	128.7		
Total	202	165,855.1				

Main Effects Plot for Perpendicularity of vertical surfaces S to P1
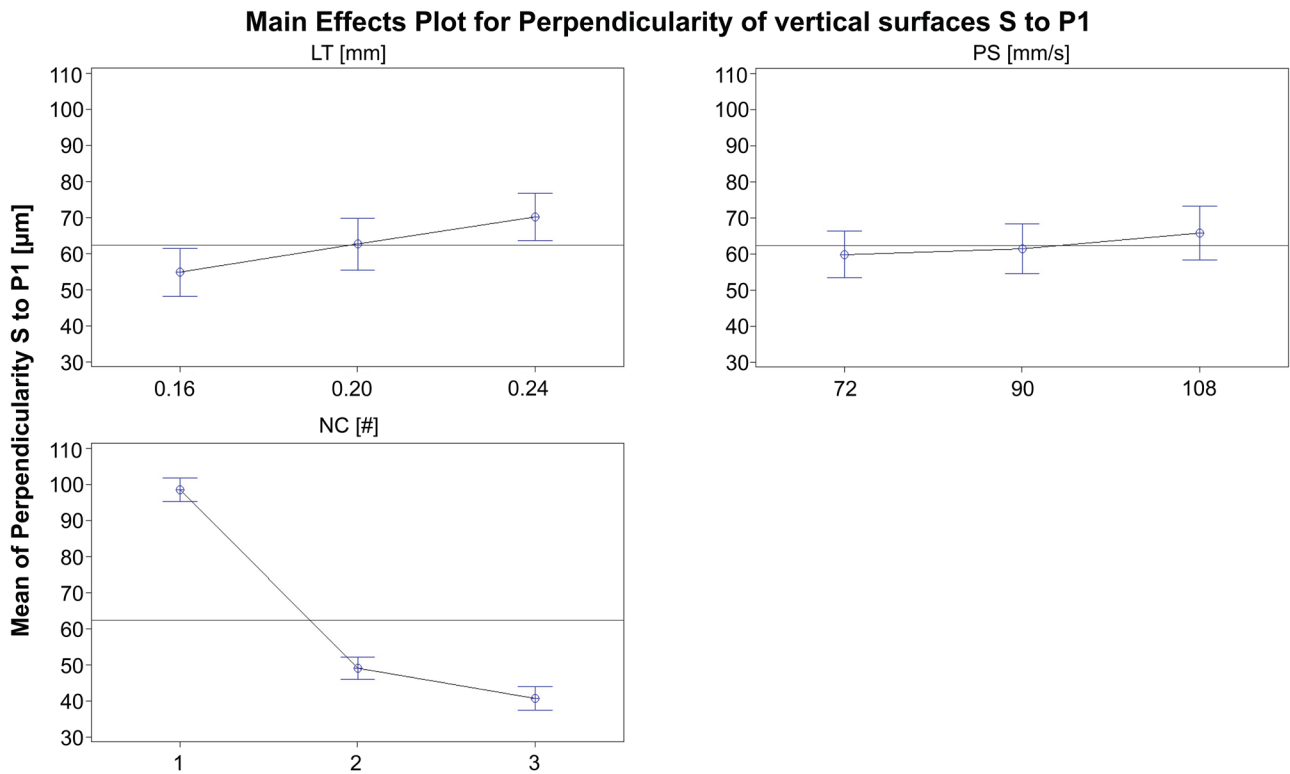
Fig. 25 Main effects plot for $PERP_{SxP1}$

$$PP_\% = 100 \cdot \frac{PP_i - PP_{low}}{PP_{high} - PP_{low}} \tag{11}$$

where

- $PP_\%$ is the normalized process parameter (*LT*, or *PS*, or *NC*),

- PP_i is the value of the process parameter to be normalized,
- PP_{low} and PP_{high} are the low and high value of the process parameter (Table 4), respectively.

Geometric deviations and time have been normalized using Eq. (12):

Fig. 26 Probability plot of printing times (in s) resulting from normality test

Main Effects Plot for Printing Times

Fig. 27 Main effects plot for printing times

$$DT_\% = 100 \frac{DT_i}{DT_{max}} \tag{12}$$

where

- $DT_\%$ is the normalized geometric deviation or time,
- DT_{max} is its maximum overall value, and
- DT_i is the value to be normalized.

Table 17 Comparison of experimental and calculated values of geometric deviations
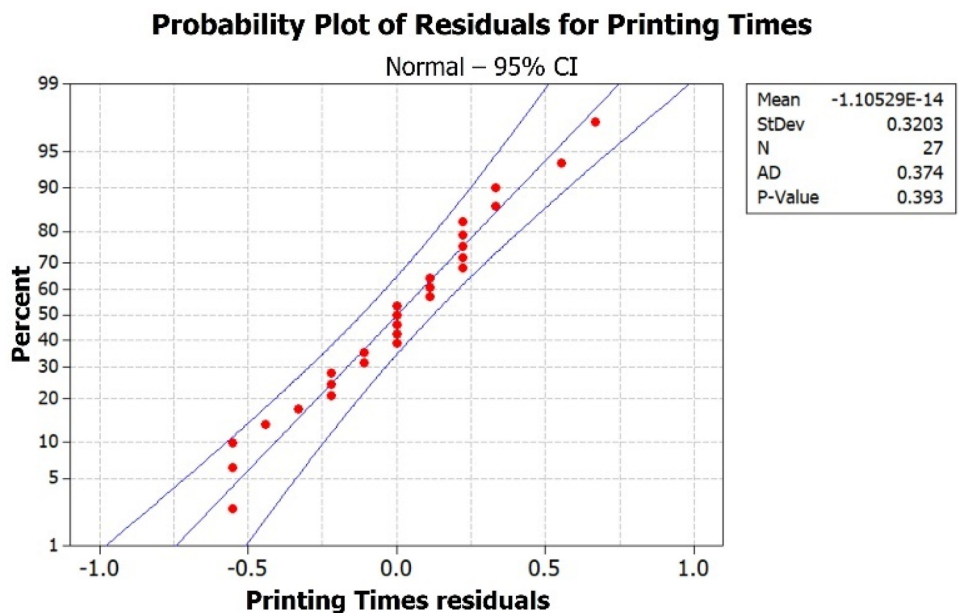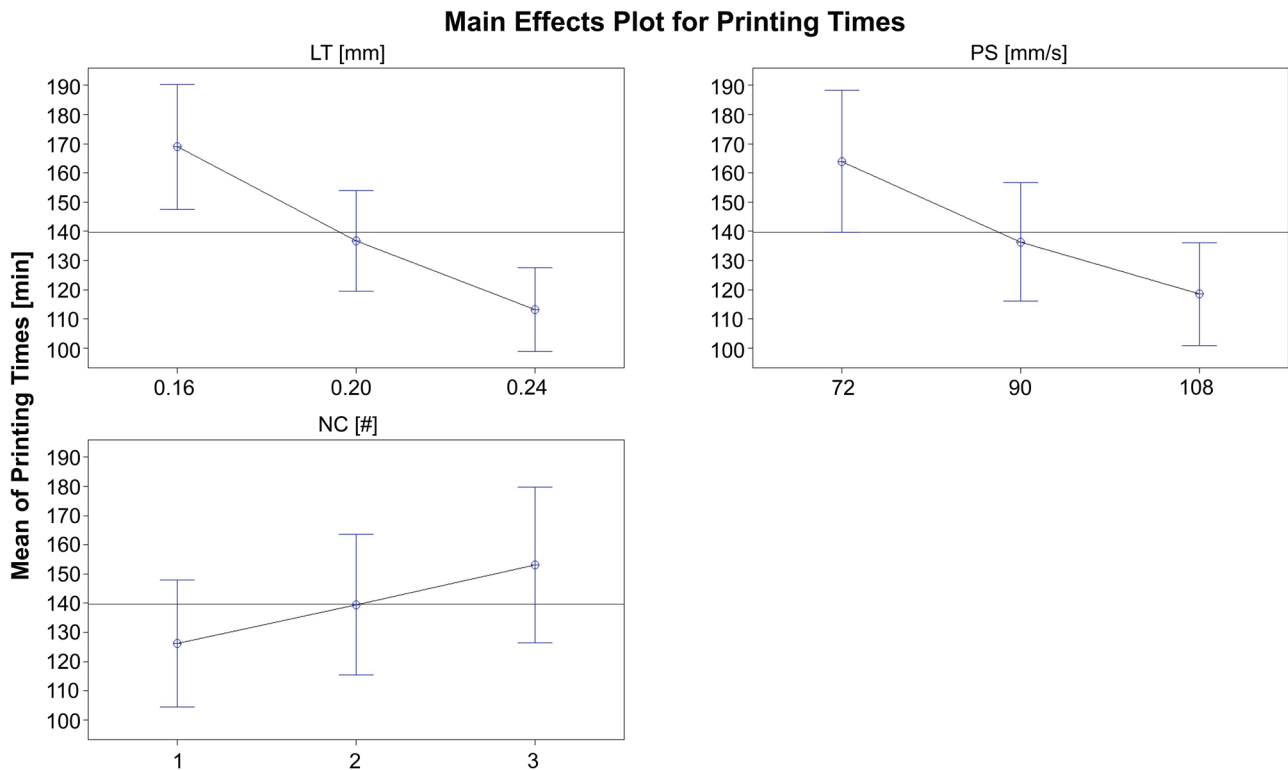
Geometric deviation	e_{min} [mm]	e_{MAX} [mm]	$e_\%$
$FLAT_P$	0.0001	0.0181	16
$FLAT_S$	0.0013	0.0225	22
$FLAT_I$	0.0002	0.0197	11
CYL_{Cv}	0.0009	0.0257	5
CYL_{Ci}	0.0001	0.0363	16
$CONC_{CxCy}$	0.0042	0.0870	11
PAR_{PxPy}	0.0002	0.0962	23
PAR_{SxSy}	0.0014	0.0414	14
$PERP_{SxP1}$	0.0002	0.0210	16

The applied normalization permits to represent all the response parameters, namely, geometric deviations and *PT*, in the same plot to evaluate the influence of process parameters on them clearly. Figures 29, 30, and 31 report the behavior of the normalized response parameters as a function of normalized *LT*, *PS*, and *NC*, respectively. In these plots, the dotted lines represent the evolution trend of responses, and their agreement with the previously depicted main effects plot is observable. In addition to this, the slope coefficient *sl* of each trend line is indicated.

The significance of the process parameters' influence can be assessed by the comparison of *sl*. In particular, the higher the absolute value of *sl*, the higher the significance in which it is influenced. Moreover, a negative value of *sl* indicates a geometric deviation or a *PT* reduction, meaning an improved quality, or a quicker process, respectively, while the opposite applies in case of a *sl* positive value.

The values of *sl* are summarized in Table 20, where, for a quicker identification of the most influencing parameters, the background of each cell is colored in a scale from light to dark gray, as a function of the *sl* absolute value. Through this table, an overall ranking of importance of the effects of process parameters on quality and *PT* can be assessed.

Table 18 ANOVA for printing times

Analysis of variance for printing times						
Source	DOF	Seq SS	Adj SS	Adj MS	F	p
LT	2	14,112.9	14,112.9	7056.4	339.80	<0.001
PS	2	9433.6	9433.6	4716.8	227.13	<0.001
NC	2	3226.9	3226.9	1613.4	77.69	<0.001
Error	20	415.3	415.3	20.8		
Total	26	27,188.7				

Table 19 Percentage error for the printing times

Test	$e_\%$	Test	$e_\%$	Test	$e_\%$
1	1.03	10	4.48	19	2.06
2	3.76	11	4.63	20	12.60
3	3.68	12	1.68	21	1.51
4	1.75	13	2.95	22	1.17
5	6.44	14	5.07	23	6.83
6	1.38	15	1.14	24	3.74
7	1.02	16	2.93	25	1.93
8	0.15	17	1.03	26	1.28
9	1.54	18	0.05	27	1.35

Fig. 28 Evolution of geometric deviations as a function of printing time
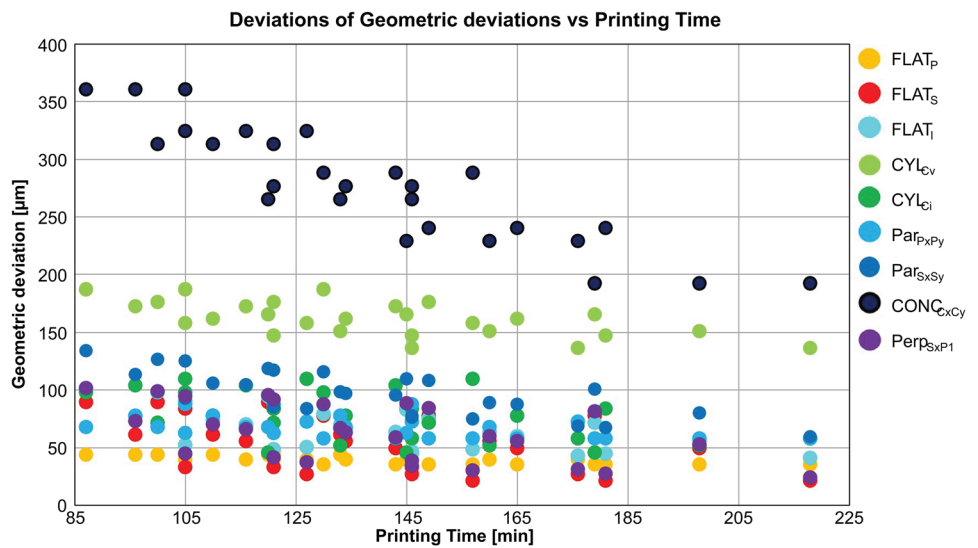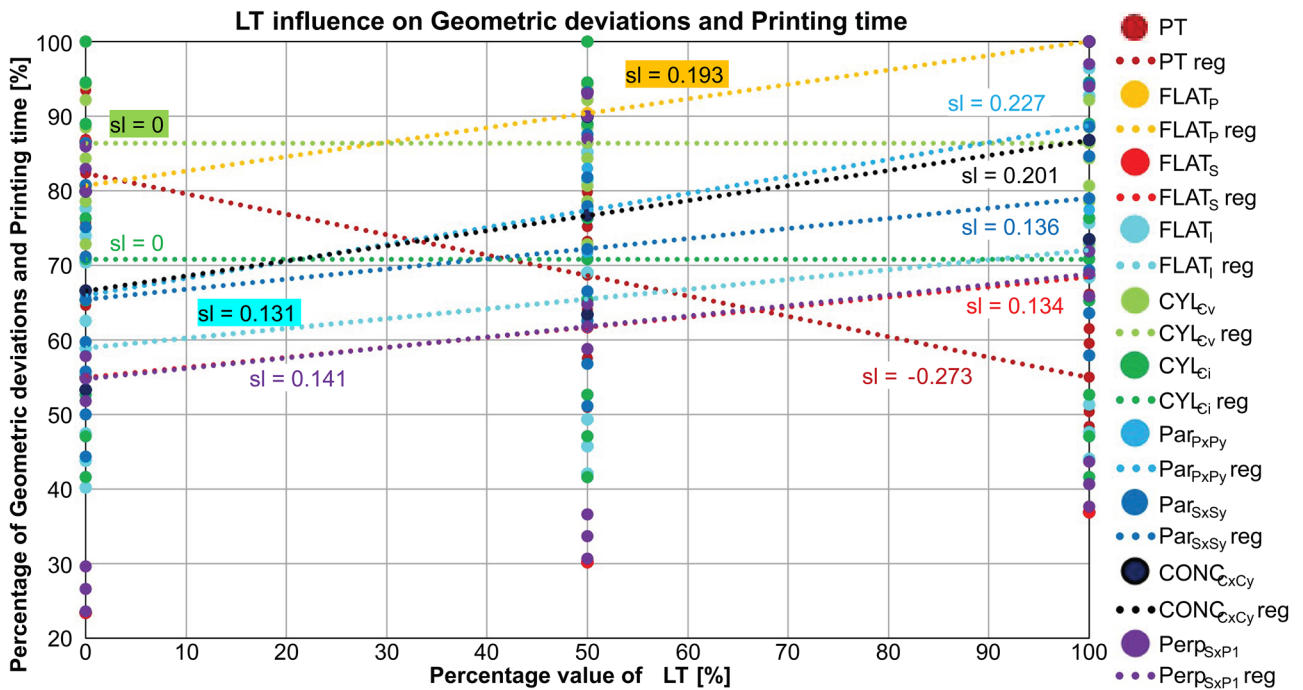
Fig. 29 Influence of layer thickness on geometric deviations and printing time
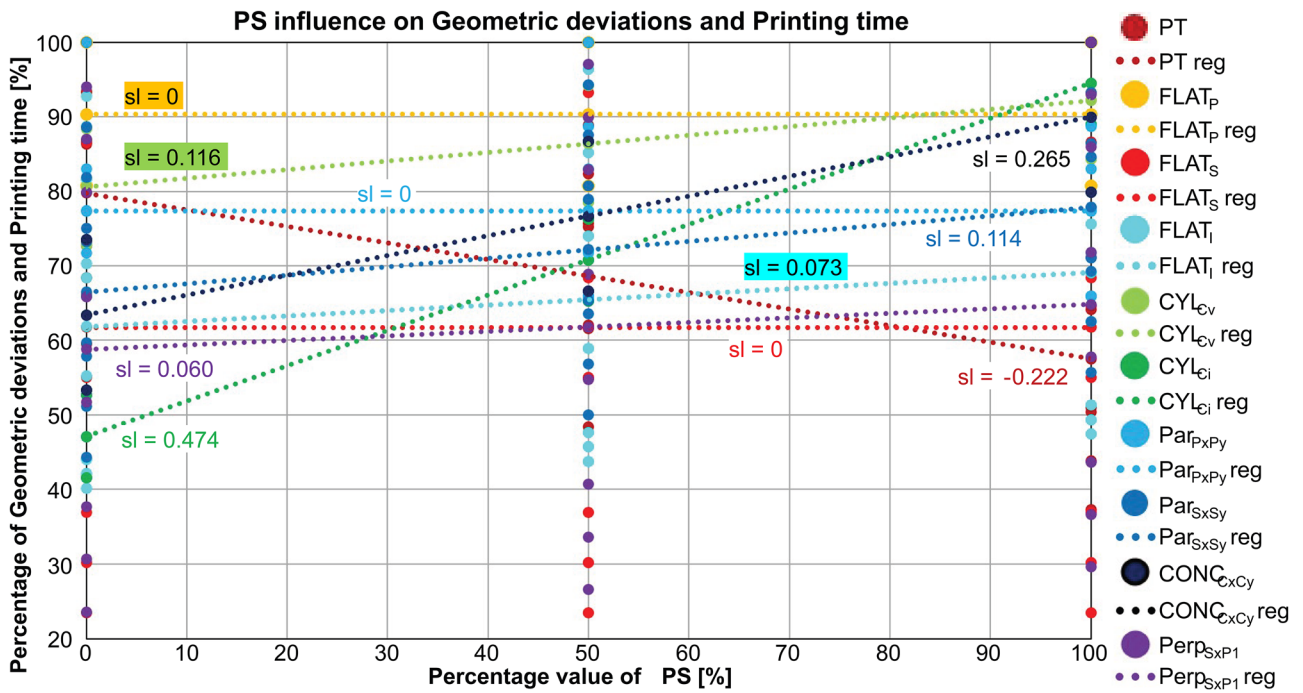
Fig. 30 Influence of printing speed on geometric deviations and printing time
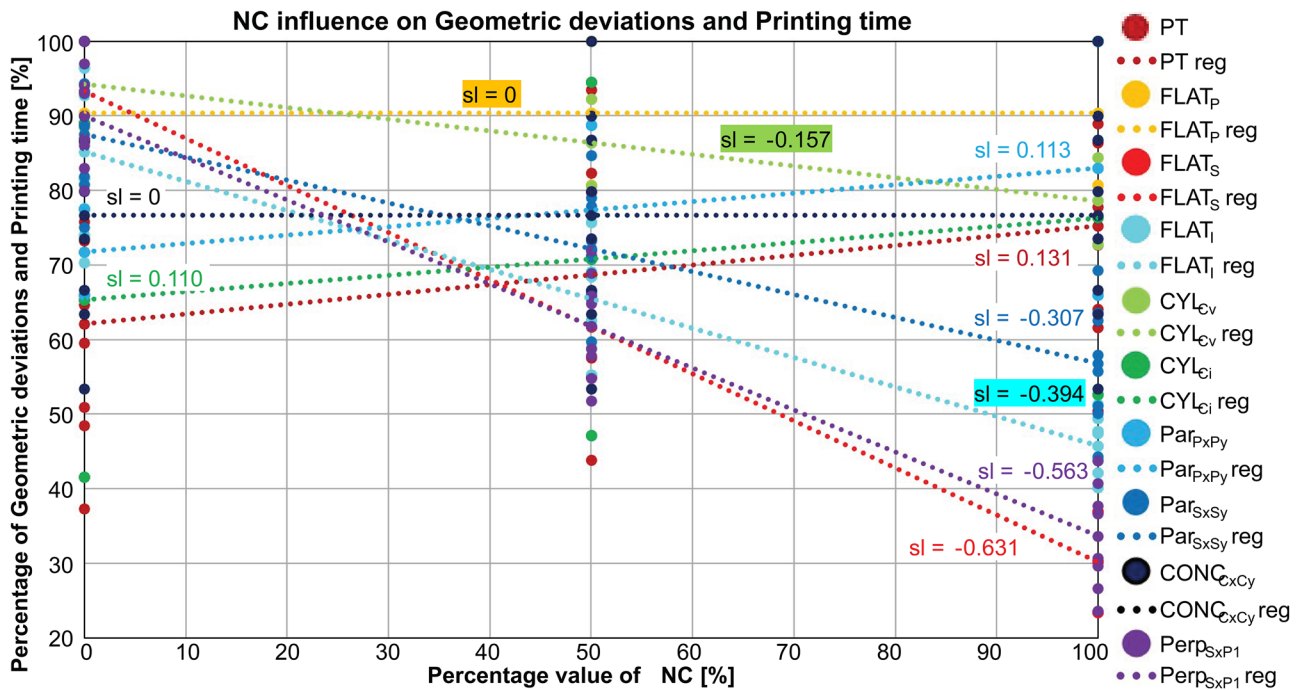
Fig. 31 Influence of number of contours on geometric deviations and printing time

Table 20 Values of the slopes of the curves of influence of process parameters on quality and printing time

Geometric Deviations and Printing Time	Process parameters		
	LT	PS	NC
PT	-0.273	-0.222	0.131
FLAT_P	0.193	0.000	0.000
FLAT_S	0.134	0.000	-0.631
FLAT_I	0.131	0.073	-0.394
CYL_Cv	0.000	0.116	-0.157
CYL_Ci	0.000	0.474	0.110
Par_PxPy	0.227	0.000	0.113
Par_SxSy	0.136	0.114	-0.307
CONC_CxCy	0.201	0.265	0.000
Perp_SxP1	0.141	0.060	-0.563

Overall, the most affecting parameter results to be *NC*, followed by *LT* and then *PS*.

Once the weight of importance of the process parameters on the quality and time responses is identified, in order to select the best combination of the values of the process parameters, an optimization process was performed. The target of the optimization was to maximize the accuracy of the product considering the possibility of reducing the production time as well. Under these assumptions, the optimization setup concerned the minimization of all the geometric deviations and *PT*. The results of the optimization phase are visible in Fig. 32. In the first four rows, the high and low values of process parameters are reported in black, while their optimized values are highlighted in red under the indication "Cur." The first column of the subsequent rows shows the examined response; its estimated value, as a function of the regression models of Eqs. from (1) to (10), in the correspondence of the optimized process, in blue; and its desirability. The latter marks the closeness of the estimated value of the response with respect to the desired one. In practice, since the objective of the optimization is the response minimization, as indicated by the term "Minimum" in Fig. 32, this means that a desirability value equal to 1 represents a minimized response, while the response gets worse if the value becomes lower. In the right hand part of Fig. 32, the evolution trends of the responses, while the process parameters increase, are depicted with black lines. Also in this case, the agreement of these trends with the ones of Figs. 29, 30, and 31 is confirmed. The red vertical lines indicate the values of the optimized process parameters. Their intersection with the trend lines indicates the position of the blue dashed lines that are the graphical depiction of the optimized responses.

The optimized values of the process parameters are *LT* equal to 0.16 mm, the lowest *LT* value, *PS* equal to 89.97 mm/s, close to the mid-range value of *PS*, and *NC* equal to 2.92, close to the highest *NC* value. These results underline again the main importance of the influence of *LT* and *NC* as asserted in Table 20. The optimized *PT* results to be equal to 180 min, which is not properly minimized as it corresponds to the 80% of the maximum *PT*. This is correlated to the fact that, during the optimization phase, higher importance has been given to the final quality of the printed component. As previously observed in Fig. 28, the quality improves when the *PT* increases. A minimization of the *PT* surely reduces the AM machine hourly costs but, at the same time, leads to the worsening of printed part quality, which implies mandatory costly and time-consuming post-process operations potentially overcoming the previously saved expenses. In this perspective, a *PT* of 180 min can be deemed acceptable as it provides for the highest achievable quality in the explored range of process parameters.
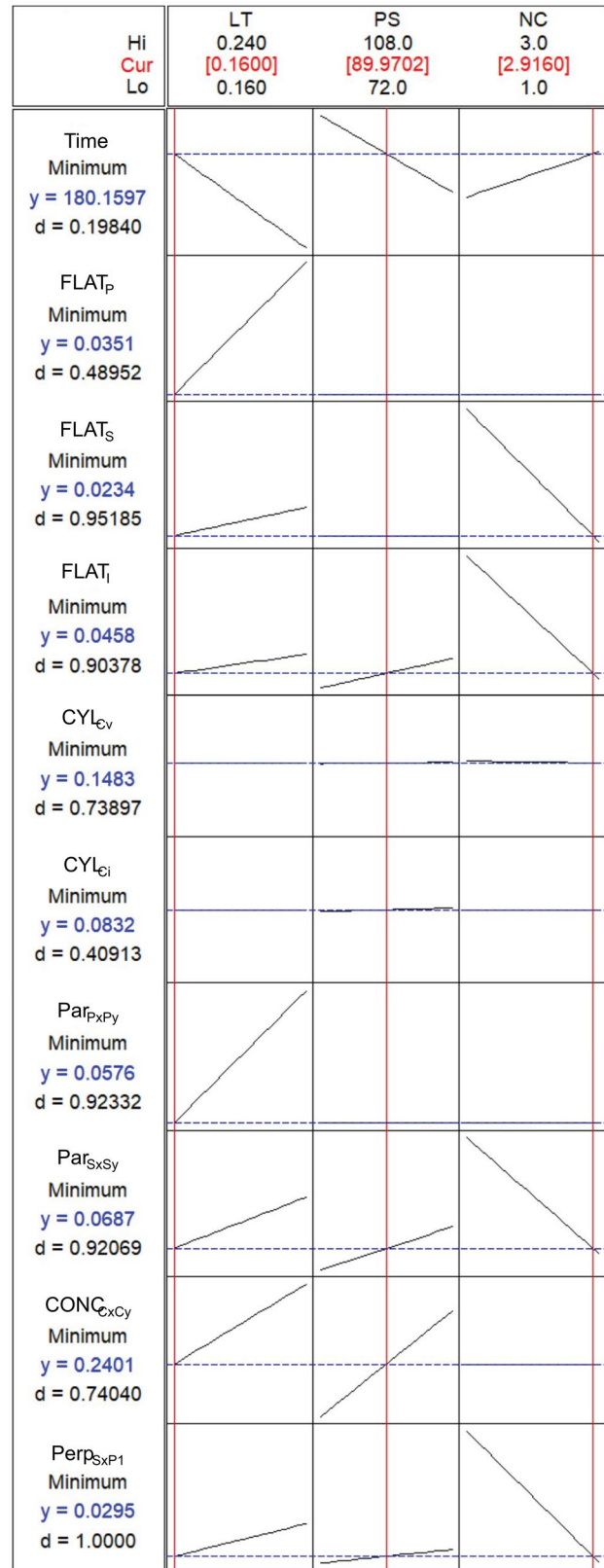

Fig. 32 Results of the optimization process

5 Conclusions

It is acknowledged that AM allows the extension of the design space, especially in terms of shape freedom. However, the quality and performances of AM-ed parts are simultaneously affected by both the design itself and the chosen process parameters for its concrete realization. Optimizing the interdependent design and fabrication is also a prerogative of the FDM technology [72], which is both established for RP scopes and increasingly used for the manufacturing of end products. In this context, the literature has so far failed to address the effect of process parameters on geometric accuracy, despite GD&T is considered among the relevant fields for the standardization of AM processes [68]. Contextually, the achievement of quality characteristics is commonly counterbalanced by long 3D printing times (the results shown in Sect. 4 are of no exception), which should be also considered in optimization tasks.

The present paper represents an original attempt to widely address the role played by FDM process parameters in geometric accuracy, while contextually considering the process duration. To this scope, the design of experiments has included a full factorial combination of three considered process parameters manipulated in three levels. Five typologies of geometric deviations and the printing time have been used as response variables. For all these typologies, the paper reports results, statistical analysis, and the authors' comments (Sect. 4) whenever they believed that the effects of process parameters on accuracy could be explained plausibly. Evidently, the statistical analyses provided significant correlations, but those cannot be interpreted as cause-effect relationships. This implies that the authors' interpretation can be challenged by other scholars or experts. Relevant similarities and differences with past studies have been highlighted as well in Sect. 4. The results include a proposal to optimize process parameters to target accuracy and time, although the former was prioritized. From a methodological viewpoint, this optimization is a plain attempt to balance quality and time aspects in a FDM process, to be possibly replicated with different quality factors, priorities, and, possibly, mechanical performances.

Within the results, the potential effect of the chosen process parameters on geometric accuracy hypothesized by the authors (see Sect. 4.4) has been confirmed. The *NC*, which has been poorly investigated in previous studies

concerning the quality of FDM 3D-printed parts (see Table 1), turned to be the most impacting factor overall. Nevertheless, it has to be noted that the effect of the process parameters is uneven if the different kinds of geometric deviations are considered. This calls into the question the need to consider each situation separately based on the design of the part and the critical geometric tolerances—the 3D-printed part used here was designed for experimental purposes only.

In addition to this, the outcomes highlight that the position of surfaces is a further factor to be considered, e.g., the investigated process parameters affected differently the flatness of horizontal and vertical surfaces. The numerous relations that have been studied offer abundant insights, but the data made available lends itself to even more detailed analyses, e.g., differences of effects across planar horizontal surfaces according to their distance from the printing plane.

The research is nevertheless subjected to several limitations, which are considered unavoidable since the topic has been practically neglected hitherto. Markedly, a number of factors should be considered that could invalidate the presented results if a similar study is replicated. These factors include a number of aspects or parameters chosen in a partially arbitrary way or for convenience; examples follow:

- The geometry and size of the part; here, it can be however hypothesized that the topology would affect process times more than the effects of process parameters on geometric accuracy.
- The material used (PLA).
- The 3D printing FDM device.

As the number of possibly manipulated process parameters is plainly larger than the set of the chosen ones (see Table 1), the most critical parameter for geometric accuracy cannot be properly identified. Future studies should aim to contextually investigate different parameters and validate the effects of the already studied ones. In this respect, the authors are available to share additional materials, e.g., the CAD model of the used part, to allow the replication of the experiment by other research groups. Authors' future work includes akin studies focusing on materials used in FDM and characterized by better mechanical performances, e.g., fiber-reinforced filaments.

Appendix A

Fig. 33 A complete 2D CAD model of the part to be printed (top view and sectioned front view)
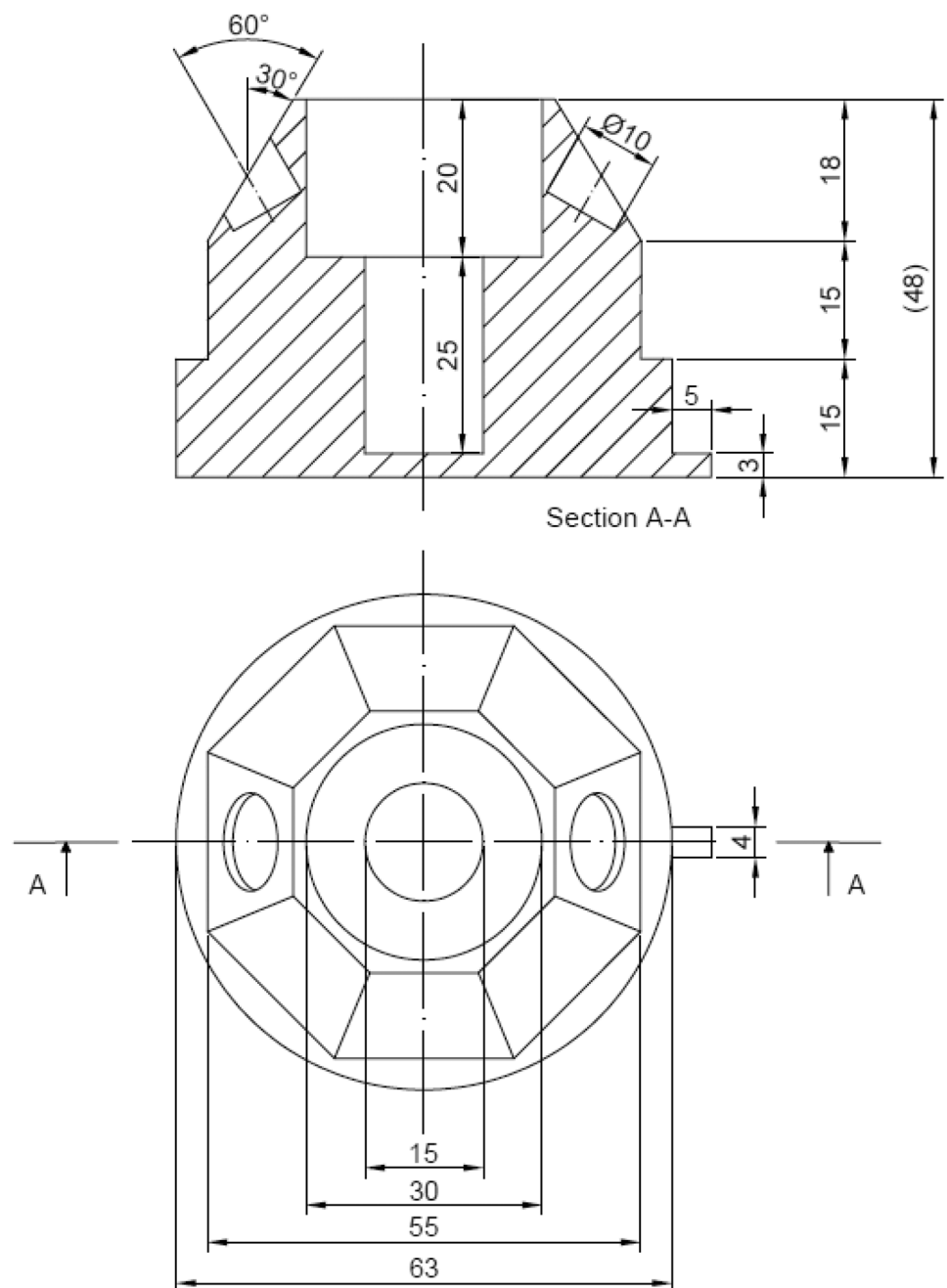
Appendix B

In this appendix, all the measurements of the acquired geometric deviations, expressed in [μm], are reported from Tables 21 to 28

Appendix B1

Table 21 Experimental values for flatness of horizontal surfaces $FLAT_P$

Test no.	$FLAT_{P1}$	$FLAT_{P2}$	$FLAT_{P3}$
1	12.0	27.6	39.7
2	20.8	36.3	48.0
3	24.4	45.9	23.3
4	20.8	21.5	29.8
5	40.6	34.4	27.8
6	31.3	59.4	44.5
7	48.2	56.2	17.7
8	19.8	51.1	22.5
9	36.7	18.7	42.3
10	62.4	28.4	208.6
11	25.7	43.2	45.4
12	59.0	29.3	237.5
13	26.9	49.3	31.8
14	43.0	51.2	46.8
15	70.1	26.0	152.1
16	87.6	54.9	35.0
17	12.5	61.1	39.5
18	52.0	37.5	39.5
19	32.8	30.1	85.7
20	21.6	29.3	368.0
21	27.8	45.4	65.2
22	47.1	24.9	331.2
23	46.5	43.3	60.7
24	40.9	44.3	69.8
25	41.5	31.0	51.3
26	38.6	24.2	312.9
27	54.6	32.9	49.9

Appendix B2

Table 22 Experimental values for flatness of vertical surfaces $FLAT_S$

Test no.	$FLAT_{S1}$	$FLAT_{S2}$	$FLAT_{S3}$	$FLAT_{S4}$	$FLAT_{S5}$	$FLAT_{S6}$	$FLAT_{S7}$	$FLAT_{S8}$
1	73.6	81.8	89.7	104.8	110.7	53.3	85.3	63.2
2	13.4	26.3	25.8	40.9	44.8	29.8	23.1	45.3
3	72.2	67.2	72.6	95.3	91.5	82.5	86.0	89.4
4	18.1	26.6	29.1	30.2	26.5	40.8	41.6	29.9
5	14.8	35.1	26.9	25.5	21.0	21.2	25.5	44.4
6	80.9	74.8	72.4	103.8	108.2	101.4	86.5	88.8
7	13.5	33.2	27.9	26.8	21.4	24.7	21.9	40.4
8	33.9	26.9	24.0	28.8	29.8	29.8	33.1	37.0
9	28.7	46.4	35.6	40.0	34.5	53.4	36.7	41.1
10	18.9	20.7	40.5	56.5	44.0	43.6	43.1	50.0
11	82.4	96.3	85.9	115.6	107.7	100.1	111.5	89.1
12	34.5	32.4	48.9	39.8	54.3	30.5	32.8	57.6
13	82.5	87.0	93.0	102.5	110.8	98.3	76.1	91.9
14	29.3	30.2	43.0	36.8	37.3	36.1	24.4	33.3
15	29.5	34.4	34.6	42.6	52.0	37.2	45.9	52.0
16	22.3	46.6	52.0	43.5	34.1	40.1	29.6	43.7
17	78.9	88.4	92.3	86.8	102.1	127.2	116.4	107.7
18	36.8	28.4	35.0	25.1	24.5	23.4	31.9	44.2
19	25.3	48.4	58.2	57.4	47.9	57.1	38.8	68.8
20	79.1	88.9	75.8	102.0	118.3	91.7	97.6	96.3
21	31.4	38.1	53.4	54.4	46.0	42.8	36.3	50.9
22	77.8	86.0	76.0	92.0	110.1	98.0	85.8	106.7
23	34.9	36.1	51.0	38.3	36.6	58.9	57.6	34.9
24	31.5	21.6	23.9	40.5	36.7	46.1	38.9	41.9
25	27.3	24.4	40.1	44.0	44.7	46.2	45.1	39.2
26	82.5	84.8	77.0	110.1	116.3	107.7	117.8	93.9
27	41.1	47.1	53.7	51.2	48.1	65.5	57.8	59.1

Appendix B3

Test no.	$FLAT_{I1}$	$FLAT_{I2}$	$FLAT_{I3}$	$FLAT_{I4}$	$FLAT_{I5}$	$FLAT_{I6}$	$FLAT_{I7}$	$FLAT_{I8}$
1	68.5	63.2	80.2	91.7	32.6	95.5	76.8	70.9
2	16.2	35.9	45.5	47.6	39.7	52.7	41.9	42.9
3	62.4	84.5	88.8	86.6	24.4	91.0	72.1	55.4
4	52.8	59.0	68.3	62.1	56.5	78.4	54.3	37.4
5	60.0	40.3	71.7	62.1	43.9	42.9	40.6	55.8
6	92.7	64.0	93.6	83.4	43.8	88.0	91.1	86.1
7	110.9	60.9	57.9	53.5	44.1	50.1	40.0	46.6
8	67.0	58.3	45.9	32.6	31.1	50.1	46.8	66.3
9	162.2	47.7	57.5	56.6	28.0	78.5	56.9	45.7
10	32.1	61.4	53.9	75.2	37.4	62.1	46.5	45.8
11	66.3	95.7	112.6	109.5	30.1	119.2	89.8	77.4
12	27.7	48.8	79.1	56.6	25.0	51.5	63.5	50.4
13	76.5	70.4	101.8	106.0	41.3	111.3	62.7	91.0
14	41.2	44.1	57.1	37.2	39.6	40.9	45.4	56.0
15	46.3	65.7	60.2	71.4	33.0	80.2	44.5	54.9
16	67.9	75.9	39.7	63.6	41.2	54.0	28.0	48.7
17	67.2	117.3	108.1	125.1	34.0	109.3	89.3	104.5
18	40.8	59.1	67.5	60.5	36.1	40.9	48.3	53.4
19	58.6	88.3	86.0	75.6	45.8	66.6	89.0	59.5
20	87.1	127.2	130.6	86.8	56.1	115.2	92.4	155.1
21	45.5	45.1	39.1	58.9	59.1	38.1	47.5	75.0
22	97.7	116.5	120.8	95.7	35.9	132.1	74.1	127.8
23	47.5	57.3	56.1	94.3	50.0	60.5	44.3	66.1
24	71.8	56.7	44.2	35.9	26.9	50.5	43.5	71.5
25	40.4	66.9	58.5	73.3	50.4	70.3	50.1	63.5
26	80.1	114.6	104.3	129.5	35.9	141.1	73.7	126.5
27	41.6	50.8	60.5	71.0	48.9	72.6	49.8	66.0

Table 23 Experimental values for flatness of inclined surfaces $FLAT_I$

Appendix B4

Table 24 Experimental values for cylindricity CYL_C

Test no.	CYL_{C1}	CYL_{C2}	CYL_{C3}	CYL_{C4}	CYL_{C5}
1	123.7	133.0	256.1	58.0	65.7
2	101.1	117.1	204.6	39.9	31.4
3	131.7	165.6	279.1	72.5	52.2
4	112.0	134.3	241.8	51.7	43.2
5	134.3	124.1	171.1	64.5	32.9
6	89.5	155.4	239.1	142.9	47.0
7	104.9	146.1	188.4	125.4	69.0
8	100.4	125.0	217.8	85.5	76.4
9	69.7	130.0	243.9	133.0	79.1
10	122.6	150.3	218.5	36.2	54.4
11	135.2	153.2	259.7	76.6	59.0
12	114.4	99.6	208.3	70.0	18.4
13	110.9	118.9	249.6	74.9	51.6
14	126.0	133.4	199.4	84.4	86.7
15	114.8	188.7	256.0	125.0	67.5
16	94.1	167.9	207.0	141.0	110.3
17	147.0	191.2	239.0	154.8	50.8
18	129.4	111.1	196.9	63.9	51.6
19	110.8	210.7	186.3	174.0	52.8
20	115.6	201.0	230.3	131.7	67.7
21	106.1	104.0	188.4	75.1	37.6
22	137.0	139.5	250.3	72.5	59.6
23	95.2	188.5	260.3	175.7	76.3
24	123.7	142.8	176.6	128.3	104.0
25	87.2	161.3	230.8	69.3	66.9
26	130.3	152.6	232.7	107.4	57.5
27	72.6	148.4	184.4	53.1	52.5

Appendix B5

Table 25 Experimental values for concentricity $CONC_{CxCy}$

Test no.	$CONC_{C1C3}$	$CONC_{C2C1}$	$CONC_{C2C3}$
1	331.8	294.2	221.1
2	237.6	234.0	173.5
3	481.6	284.4	288.2
4	284.3	177.8	217.8
5	451.5	195.9	255.6
6	245.1	253.8	221.4
7	338.3	307.0	211.1
8	276.2	197.9	186.0
9	317.6	243.4	213.1
10	228.9	296.8	196.3
11	359.8	294.8	214.4
12	182.5	195.5	129.0
13	248.4	171.5	216.2
14	435.7	273.8	238.2
15	220.5	401.2	259.1
16	288.6	356.8	244.2
17	395.9	475.2	258.5
18	298.4	246.7	183.9
19	522.8	473.8	318.1
20	442.3	531.5	270.3
21	323.6	265.1	230.4
22	285.5	295.2	210.7
23	325.3	420.6	329.9
24	239.4	336.2	209.8
25	464.4	361.8	237.8
26	403.4	341.0	229.2
27	188.4	347.9	148.0

Appendix B6

Table 26 Experimental values for parallelism of horizontal surfaces PAR_{PxPy}

Test no.	PAR_{P2P1}	PAR_{P3P1}	PAR_{P3P2}
1	44.9	46.1	37.9
2	63.3	55.5	68.1
3	54.5	37.6	24.8
4	37.1	46.3	39.5
5	56.0	44.0	47.6
6	91.2	44.1	64.5
7	85.6	63.0	27.9
8	78.1	73.2	33.7
9	42.9	45.3	50.4
10	60.4	250.5	232.5
11	45.5	65.9	73.9
12	40.9	303.2	313.7
13	63.9	33.4	44.2
14	59.4	47.4	61.8
15	36.8	170.4	163.2
16	72.8	56.0	43.4
17	104.7	50.3	57.8
18	38.2	57.6	64.3
19	69.0	99.3	104.7
20	37.9	390.4	383.7
21	49.5	92.0	87.1
22	46.1	346.3	362.5
23	94.5	98.3	77.8
24	66.7	109.4	85.9
25	45.0	73.5	58.1
26	32.6	353.5	359.6
27	39.5	80.8	86.0

Appendix B7

Table 27 Experimental values for parallelism of vertical surfaces PAR_{SxSy}

Test no.	PAR_{S5S1}	PAR_{S6S2}	PAR_{S7S3}	PAR_{S8S4}
1	99.9	94.2	131.1	80.9
2	70.7	41.4	89.1	62.9
3	147.5	118.7	151.7	116.5
4	61.1	62.7	111.9	60.5
5	59.9	25.7	69.1	98.2
6	125.1	158.3	121.9	117.5
7	67.7	44.7	89.5	146.3
8	67.4	61.5	113.1	87.9
9	46.0	66.0	110.2	77.0
10	60.4	48.1	108.3	76.5
11	128.0	100.5	163.4	100.4
12	83.4	43.7	54.3	67.4
13	104.7	112.0	126.2	96.3
14	61.5	45.9	81.1	88.3
15	81.5	61.2	97.0	70.6
16	71.9	62.4	113.9	109.8
17	144.3	142.0	158.9	136.7
18	67.3	23.6	92.2	89.0
19	178.4	131.5	185.2	191.1
20	142.5	136.1	154.6	113.5
21	116.0	76.3	108.7	120.5
22	106.4	107.0	140.4	124.8
23	72.2	99.4	132.4	68.6
24	81.9	53.4	120.0	89.1
25	78.3	73.3	125.6	84.3
26	129.5	114.4	180.7	99.2
27	105.3	106.0	141.1	107.7

Appendix B8

Table 28 Experimental values for perpendicularity of vertical surfaces with respect to P1 $PERP_{SxP1}$

Test no.	$PERP_{S1P1}$	$PERP_{S2P1}$	$PERP_{S3P1}$	$PERP_{S4P1}$	$PERP_{S5P1}$	$PERP_{S6P1}$	$PERP_{S7P1}$	$PERP_{S8P1}$
1	92.3	76.6	96.5	102.6	116.7	56.3	89.6	63.2
2	36.0	33.7	38.1	49.1	47.8	28.8	45.9	49.6
3	84.6	79.2	70.1	92.4	99.9	99.0	100.2	92.2
4	31.7	31.2	29.6	29.0	37.6	58.1	55.3	53.6
5	34.0	41.9	36.5	27.2	27.2	21.2	25.0	48.1
6	106.1	81.6	87.1	104.0	99.6	113.9	101.5	93.5
7	23.9	35.0	34.1	26.8	30.2	31.4	21.9	41.4
8	59.4	34.1	27.6	29.0	31.0	29.7	36.8	42.4
9	27.0	49.3	35.7	45.4	36.7	56.3	56.4	55.7
10	34.2	19.7	39.1	53.7	43.4	43.5	70.2	83.6
11	104.8	91.6	84.2	118.7	114.4	105.7	107.2	90.5
12	48.6	33.3	51.3	38.4	56.3	33.6	55.5	68.3
13	83.2	92.5	113.3	98.1	103.5	95.6	87.0	94.5
14	40.2	34.5	51.1	40.7	44.3	38.6	35.2	31.1
15	37.6	34.8	34.7	52.0	64.1	55.3	61.9	56.9
16	25.6	46.6	51.3	38.8	34.1	44.7	52.8	50.1
17	113.6	93.5	89.5	98.1	108.1	135.6	129.9	113.6
18	35.9	30.8	41.4	25.9	24.5	24.1	33.1	49.8
19	55.9	94.7	84.5	81.3	90.0	75.0	57.8	73.2
20	74.4	92.2	82.5	104.1	129.1	105.1	129.8	102.7
21	31.4	53.4	75.8	78.0	66.4	55.4	35.4	50.5
22	77.8	90.6	90.5	92.6	109.9	92.8	94.9	106.5
23	45.8	46.8	57.9	53.5	49.8	75.9	76.2	52.6
24	36.3	51.9	26.6	44.8	37.5	47.3	49.4	42.6
25	41.4	33.2	48.4	45.6	56.0	53.8	71.3	73.4
26	115.7	90.8	82.9	107.1	107.7	115.5	141.7	107.1
27	37.5	49.0	55.4	62.4	72.9	89.5	68.0	70.4

Availability of data and material The authors declare that there are not restrictions in the availability of data and material.

Declarations

Competing interests The authors declare no competing interests.

References

1. Jiang J, Hu G, Li X, Xu X, Zheng P, Stringer J (2019) Analysis and prediction of printable bridge length in fused deposition modelling based on back propagation neural network. Virtual Phys Prototyp 14(3):253–266. https://doi.org/10.1080/17452759.2019.1576010

2. Borgianni Y, Maccioni L, Basso D (2019) Exploratory study on the perception of additively manufactured end-use products with specific questionnaires and eye-tracking. J Interact Des Manuf. Article in press, Int. https://doi.org/10.1007/s12008-019-00563-w

3. Jiang J, Lou J, Hu G (2019) Effect of support on printed properties in fused deposition modelling processes. Virtual Phys Prototyp 14(4):308–315. https://doi.org/10.1080/17452759.2019.1568835

4. Zaman UK, Boesch E, Siadat A, Rivette M, Baqai AA (2019) Impact of fused deposition modeling (FDM) process parameters on strength of built parts using Taguchi's design of experiments. Int J of Adv Manuf Technol 101(5):1215–1226. https://doi.org/10.1007/s00170-018-3014-6

5. Rochlitz B, Pammer D (2017) Design and analysis of 3D printable foot prosthesis. Period Polytech Mech Eng 61(4):282–287. https://doi.org/10.3311/PPme.11085

6. Chen H, Yang X, Chen L, Wang Y, Sun Y (2016) Application of FDM three-dimensional printing technology in the digital manufacture of custom edentulous mandible trays. Sci Rep 6(1):1–6. https://doi.org/10.1038/srep19207

7. Peng A, Xiao X, Yue R (2014) Process parameter optimization for fused deposition modeling using response surface methodology combined with fuzzy inference system. Int J of Adv Manuf Technol 73(1–4):87–100. https://doi.org/10.1007/s00170-014-5796-5

8. Sood AK, Ohdar RK, Mahapatra SS (2010) Parametric appraisal of mechanical property of fused deposition modelling processed parts. Mater Des 31(1):287–295. https://doi.org/10.1016/j.matdes.2009.06.016

9. Oliveira JP, LaLonde AD, Ma J (2020) Processing parameters in laser powder bed fusion metal additive manufacturing. Mater Des 193:108762. https://doi.org/10.1016/j.matdes.2020.108762

10. Abeni A, Cappellini C, Ginestra PS, Attanasio A (2022) Analytical modeling of micro-milling operations on biocompatible Ti6Al4V titanium alloy. Proc CIRP 110:8–13. https://doi.org/10.1016/j.procir.2022.06.004

11. Ramalho A, Santos TG, Bevans B, Smoqi Z, Rao P, Oliveira JP (2022) Effect of contaminations on the acoustic emissions during wire and arc additive manufacturing of 316L stainless steel. Addit Manuf 51:102585. https://doi.org/10.1016/j.addma.2021.102585

12. Rodrigues TA, Bairrão N, Cipriano Farias FW, Shamsolhodaei A, Shen J, Zhou N, Maawad E, Schell N, Santos TG, Oliveira JP (2022) Steel-copper functionally graded material produced by twin-wire and arc additive manufacturing (T-WAAM). Mater Des 213:110270. https://doi.org/10.1016/j.matdes.2021.110270

13. Thrimurthulu KPPM, Pandey PM, Reddy NV (2004) Optimum part deposition orientation in fused deposition modeling. Int J Mach Tools Manuf 44(6):585–594. https://doi.org/10.1016/j.ijmachtools.2003.12.004

14. Huang B, Meng S, He H, Jia Y, Xu Y, Huang H (2019) Study of processing parameters in fused deposition modeling based on mechanical properties of acrylonitrile-butadiene-styrene filament. Polym Eng Sci 59(1):120–128. https://doi.org/10.1002/pen.24875

15. Anitha R, Arunachalam S, Radhakrishnan P (2001) Critical parameters influencing the quality of prototypes in fused deposition modelling. J Mater Process Technol 118(1–3):385–388. https://doi.org/10.1016/S0924-0136(01)00980-3

16. Wang CC, Lin TW, Hu SS (2007) Optimizing the rapid prototyping process by integrating the Taguchi method with the Gray relational analysis. Rapid Prototyp J 13(5):304–315. https://doi.org/10.1108/13552540710824814

17. Sood AK, Ohdar RK, Mahapatra SS (2009) Improving dimensional accuracy of fused deposition modelling processed part using grey Taguchi method. Mater Des 30(10):4243–4252. https://doi.org/10.1016/j.matdes.2009.04.030

18. Sahu RK, Mahapatra SS, Sood AK (2013) A study on dimensional accuracy of fused deposition modeling (FDM) processed parts using fuzzy logic. J Manuf Sci Prod 13(3):183–197. https://doi.org/10.1515/jmsp-2013-0010

19. Zhang Y, Chou K (2008) A parametric study of part distortions in fused deposition modelling using three-dimensional finite element analysis. Proc Institution Mech Eng Part B J Eng Manuf 222(8):959–968. https://doi.org/10.1243/09544054JEM990

20. Alafaghani A, Qattawi A, Alrawi B, Guzman A (2017) Experimental optimization of fused deposition modelling processing parameters: a design-for-manufacturing approach. Proc Manuf 10:791–803. https://doi.org/10.1016/j.promfg.2017.07.079

21. Zhang JW, Peng AH (2012) Process-parameter optimization for fused deposition modeling based on Taguchi method. Adv Mat Res 538:444–447. https://doi.org/10.4028/www.scientific.net/AMR.538-541.444

22. Xinhua L, Shengpeng L, Zhou L, Xianhua Z, Xiaohu C, Zhongbin W (2015) An investigation on distortion of PLA thin-plate part in the FDM process. Int J of Adv Manuf Technol 79(5):1117–1126. https://doi.org/10.1007/s00170-015-6893-9

23. Mohamed OA, Masood SH, Bhowmik JL (2015) Optimization of fused deposition modeling process parameters: a review of

current research and future prospects. Adv Manuf 3(1):42–53. https://doi.org/10.1007/s40436-014-0097-7

24. Galati M, Minetola P (2020) On the measure of the aesthetic quality of 3D printed plastic parts. Int J Interact Des Manuf 14(2):381–392. https://doi.org/10.1007/s12008-019-00627-x

25. Schleich B, Answer N, Mathieu L, Wartzack S (2014) Skin Model Shapes: A new paradigm shift for geometric variations modelling in mechanical engineering. Comput Aided Des 50:1–15. https://doi.org/10.1016/j.cad.2014.01.001

26. Rajan K, Samykano M, Kadirgama K, Wan Harun WS, Rahman MM (2022) Fused deposition modeling: process, materials, parameters, properties, and applications. Int J Adv Manuf Technol 120:1531–1570. https://doi.org/10.1007/s00170-022-08860-1

27. Nancharaiah T, Ranga Raju D, Ramachandra Raju V (2010) An experimental investigation on surface quality and dimensional accuracy of FDM components. Int J Emerg Technol 1(2):106–111

28. Ali F, Chowdary BV, Maharaj J (2014) Influence of some process parameters on build time, material consumption, and surface roughness of FDM processed parts: inferences based on the Taguchi design of experiments. Proc. of the 2014 IACJ/ISAM Joint International Conference, Orlando, FL, USA, pp 25–27

29. Horvath D, Noorani R, Mendelson M (2007) Improvement of surface roughness on ABS 400 polymer using design of experiments (DOE). Mater Sci Forum 561:2389–2392. https://doi.org/10.4028/www.scientific.net/MSF.561-565.2389

30. Banjanin B, Vladić G, Pál M, Dimovski V, Adamović S, Delić G (2018) Production factors influencing mechanical and physical properties of FDM printed embossing dies. 9th Int Symp Graph Eng Des. https://doi.org/10.24867/GRID-2018-p28

31. Hamel JM, Salsbury C, Bouck A (2018) Characterizing the effects of additive manufacturing process settings on part performance using approximation-assisted multi-objective optimization. Prog Addit Manuf 3(3):123–143. https://doi.org/10.1007/s40964-018-0043-5

32. Nancharaiah T (2011) Optimization of process parameters in FDM process using design of experiments Int. J Emerg Technol 2(1):100–102

33. Gurrala PK, Regalla SP (2012) Optimization of support material and build time in fused deposition modeling (FDM). App Mech Mater 110:2245–2251. https://doi.org/10.4028/www.scientific.net/AMM.110-116.2245

34. Rathee S, Srivastava M, Maheshwari S, Siddiquee AN (2017) Effect of varying spatial orientations on build time requirements for FDM process: a case study. Def Technol 13(2):92–100. https://doi.org/10.1016/j.dt.2016.11.006

35. Mahmood S, Qureshi AJ, Talamona D (2018) Taguchi based process optimization for dimension and tolerance control for fused deposition modelling. Addit Manuf 21:183–190. https://doi.org/10.1016/j.addma.2018.03.009

36. Knoop F, Schoeppner V (2017) Geometrical accuracy of holes and cylinders manufactured with fused deposition modeling. Proc 28th Ann Int Solid Freeform Fabric Symp An Additive Manuf Conf 2753–2776. https://doi.org/10.26153/tsw/16990

37. Ahn DK, Kim HC, Lee SH (2005) Determination of fabrication direction to minimize post-machining in FDM by prediction of non-linear roughness characteristics. J Mech Sci Technol 19(1):144–155. https://doi.org/10.1007/BF02916113

38. Vasudevarao B, Natarajan DP, Henderson M, Razdan A (2000) Sensitivity of RP surface finish to process parameter variation 251. Int Solid Freeform Fabric Symp. https://doi.org/10.26153/tsw/3045

39. Srivastava M, Maheshwari S, Kundra TK (2015) Virtual modelling and simulation of functionally graded material component using FDM technique. Mater Today Proc 2(4–5):3471–3480. https://doi.org/10.1016/j.matpr.2015.07.323

40. Srivastava M, Rathee S (2018) Optimisation of FDM process parameters by Taguchi method for imparting customised properties to components. Virtual Phys Prototyp 13(3):203–210. https://doi.org/10.1080/17452759.2018.1440722

41. Srivastava M, Maheshwari S, Kundra TK, Rathee S (2016) An integrated RSM-GA based approach for multi response optimization of FDM process parameters for pyramidal ABS primitives. J Manuf Sci Produc 16(3):201–208. https://doi.org/10.1515/jmsp-2016-0012

42. Phatak AM, Pande SS (2012) Optimum part orientation in rapid prototyping using genetic algorithm. J Manuf Syst 31(4):395–402. https://doi.org/10.1016/j.jmsy.2012.07.001

43. Kaveh M, Badrossamay M, Foroozmehr E, Etefagh AH (2015) Optimization of the printing parameters affecting dimensional accuracy and internal cavity for HIPS material used in fused deposition modeling processes. J Mater Process Technol 226:280–286. https://doi.org/10.1016/j.jmatprotec.2015.07.012

44. Vyavahare S, Kumar S, Panghal D (2020) Experimental study of surface roughness, dimensional accuracy and time of fabrication of parts produced by fused deposition modelling. Rapid Prototyp J 26(9):1535–1554. https://doi.org/10.1108/RPJ-12-2019-0315

45. Wan Suaidi SNS, Azizul MA, Sulaiman S, Hao TY (2020) Effect of fused deposition modelling process parameters on the quality of ABS product. J Ind Eng Innov 2(1):9. https://fazpublishing.com/jiei/index.php/jiei/article/view/43

46. Pramanik D, Mandal A, Kuar AS (2020) An experimental investigation on improvement of surface roughness of ABS on fused deposition modelling process. Mater Today: Proc 26:860–863. https://doi.org/10.1016/j.matpr.2020.01.054

47. Galetto M, Verna E, Genta G (2021) Effect of process parameters on parts quality and process efficiency of fused deposition modeling. Comput Ind Eng 156:107238. https://doi.org/10.1016/j.cie.2021.107238

48. Singh D, Singh R, Boparai KS (2020) Investigations for surface roughness and dimensional accuracy of biomedical implants prepared by combining fused deposition modelling, vapour smoothing and investment casting. Adv Mater Process Technol 1–20. https://doi.org/10.1080/2374068X.2020.1835007

49. Bähr F, Westkämper E (2018) Correlations between influencing parameters and quality properties of components produced by fused deposition modeling. Proc CIRP 72:1214–1219. https://doi.org/10.1016/j.procir.2018.03.048

50. Mendricky R, Fris D (2020) Analysis of the accuracy and the surface roughness of fdm/fff technology and optimisation of process parameters. Technical Gazette 27(4):1166–1173. https://doi.org/10.17559/TV-20190320142210

51. Camposeco-Negrete C (2020) Optimization of printing parameters in fused deposition modeling for improving part quality and process sustainability. Int J of Adv Manuf Technol 108(7):2131–2147. https://doi.org/10.1007/s00170-020-05555-9

52. Hanon MM, Zsidai L, Ma Q (2021) Accuracy investigation of 3D printed PLA with various process parameters and different colors. Mater Today: Proc 42:3089–3096. https://doi.org/10.1016/j.matpr.2020.12.1246

53. Syrlybayev D, Perveen A, Talamona D (2021) Fused deposition modelling: effect of extrusion temperature on the accuracy of print. Mater Today: Proc 44:832–837. https://doi.org/10.1016/j.matpr.2020.10.716

54. Hamza I, El Gharad Abdellah OM (2018) Experimental optimization of fused deposition modeling process parameters: a Taguchi process approach for dimension and tolerance control. Proc Int Conf Indust Eng Operations Manage 1–11

55. Salem IH (2022) Multi-objective optimization on dimensional accuracy, edge and surface quality of 3D-printed parts by fused

deposition modelling. Thesis, The American University in Cairo. AUC Knowledge Fountain. https://fount.aucegypt.edu/etds/1881

56. Schneidler J, Berry C, Barari A (2021) Improving 3D printing geometric accuracy using design of experiments on process parameters in fused filament fabrication (FFF). 14th IEEE Int Conf Indust Appl (INDUSCON) 1360–1365

57. Sheoran AJ, Kumar H (2020) Fused deposition modeling process parameters optimization and effect on mechanical properties and part quality: review and reflection on present research. Mater Today Proc 21:1659–1672. https://doi.org/10.1016/j.matpr.2019.11.296

58. Ouballouch A, Ettaqi S, Bouayad A, Sallaou M, Lasri L (2019) Evaluation of dimensional accuracy and mechanical behavior of 3D printed reinforced polyamide parts. Proc Struct Integr 19:433–441. https://doi.org/10.1016/j.prostr.2019.12.047

59. Sterca AD, Calin RA, Cristian L, Walcher EM, Bodur O, Ceclan V, Durakbasa NM (2022) Evaluation of fused deposition modeling process parameters influence on 3D printed components by high precision metrology. In: Numan Durakbasa M, Güneş Gençyılmaz M (ed) Digitizing Production Systems, 1st edn. Springer Internationl Publishing, Switzerland, pp 281–295. https://doi.org/10.1007/978-3-030-90421-0_24

60. Gómez-Gras G, Pérez MA, Fábregas-Moreno J, Reyes-Pozo G (2021) Experimental study on the accuracy and surface quality of printed versus machined holes in PEI Ultem 9085 FDM specimens. Rapid Prototyp J 27(11):1–12. https://doi.org/10.1108/RPJ-12-2019-0306

61. Kumar S, Vyavahare S, Kootikuppala J (2022) Experimental study of effect of process parameters on surface roughness and dimensional accuracy of parts fabricated by fused deposition modelling. Lect Notes Mech Eng 843–858. https://doi.org/10.1007/978-981-16-9952-8_72

62. Agarwal KM, Shubham P, Bhatia D, Sharma P, Vaid H, Vajpeyi R (2022) Analyzing the impact of print parameters on dimensional variation of ABS specimens printed using fused deposition modelling (FDM). Sens Int 3:100149. https://doi.org/10.1016/j.sintl.2021.100149

63. Pratama J, Mayanda N, Sugiyanto D (2022) Effect of extruder temperature on dimensional accuracy and surface roughness of fused deposition modeled (FDMed) PLA and PLA/wood composite. ROTASI 24(2):1–9

64. Jin YA, Li H, He Y, Fu JZ (2015) Quantitative analysis of surface profile in fused deposition modelling. Addit Manuf 8:142–148. https://doi.org/10.1016/j.addma.2015.10.001

65. Elkaseer A, Schneider S, Scholz SG (2020) Experiment-based process modeling and optimization for high-quality and resource-efficient FFF 3D printing. App Sci 10(8):2899. https://doi.org/10.3390/app10082899

66. ISO/TC 213, ISO 1101 (2017) Geometrical product specifications (GPS) — Geometrical tolerancing — tolerances of form, orientation, location and run-out. 1–145

67. ASME, Y14.46 (2017) Product definition for additive manufacturing

68. Rupal BS, Answer N, Secanell M, Qureshi AJ (2020) Geometric tolerance and manufacturing assemblablity estimation of metal additive manufacturing (AM) processes. Mater Des 194:108842. https://doi.org/10.1016/j.matdes.2020.108842

69. Ameta G, Lipman R, Moylan S, Witherell P (2015) Investigating the role of geometric dimensioning and tolerancing in additive manufacturing. J Mech Des 137(11):111401. https://doi.org/10.1115/1.4031296

70. Concli F, Maccioni L, Fraccaroli L, Cappellini C (2022) Effect of gear design parameters on stress histories induced by different tooth bending fatigue tests: a numerical-statistical investigation. Appl Sci 12(8):3950. https://doi.org/10.3390/app12083950

71. Montgomery DC, Runger GC (2018) Applied statistics and probability for engineers. Wiley, Hoboken, NJ

72. Zhang Y, Moon SK (2021) Data-driven design strategy in fused filament fabrication: status and opportunities. J Comput Des Eng 8(2):489–509. https://doi.org/10.1093/jcde/qwaa094

Publisher's Note Springer Nature remains neutral with regard to jurisdictional claims in published maps and institutional affiliations.